Earth System
Dynamics
Discussions

Tidal impacts on primary production in the North Sea

Changjin Zhao[1], Ute Daewel[1], Corinna Schrum[1]

[1]Helmholtz Centre Geesthacht, Institute of Coastal Research, Max-Planck-Str. 1, 21502 Geesthacht, Germany

Correspondence to: Changjin Zhao (changjin.zhao @hzg.de)

5   **Abstract.** This study highlights the importance of tides in controlling the spatial and temporal distributions of phytoplankton and other factors related to growth, such as nutrients and light availability. To quantify the responses of net primary production (NPP) to tidal forcing, we conducted scenario model simulations considering M_2 and S_2 tidal constituents using the physical-biogeochemical coupled model ECOSMO. The results were analysed with respect to a reference simulation without tidal forcing, with particular focus on the spatial scale of the tidally induced changes. Tidal forcing regulates the

10   mixing-stratification processes in shelf seas such as the North Sea and hence also influences ecosystem dynamics. In principle, the results suggest three different response types with respect to primary production: i) in southern shallow areas with strong tidal energy dissipation, tidal mixing dilutes phytoplankton concentrations in the upper water layers and thereby decreases NPP. Additionally, tides increase turbidity in near-coastal shallow areas, which has the potential to further hamper NPP. ii) In the frontal region of the southern North Sea, which is a transition zone between stratified and mixed areas, tidal

15   mixing infuses nutrients into the surface mixed layer and resolves summer nutrient depletion, thus sustaining the NPP during the summer season after spring bloom nutrient depletion. iii) In the northern North Sea, the NPP response to tidal forcing is limited. Additionally, our simulations indicate that spring bloom phenology is impacted by tidal forcing, leading to a later onset of the spring bloom in large parts of the North Sea and to generally higher spring bloom peak phytoplankton biomasses. By testing the related changes in stratification, light conditions and grazing pressure, we found that all three

20   factors potentially contribute to the change in spring bloom phenology with clear local differences. Finally, we also analysed the impact of the spring-neap tidal cycle on NPP. The annual mean impact of spring-neap tidal forcing on NPP is limited. However, locally, we found substantial differences in NPP either in-phase or anti-phase with the spring-neap tidal cycle. These differences could be attributed to locally different dominant factors such as light or nutrient availability during spring tides. In general, we conclude that in shallow shelf seas such as the North Sea, intensified vertical mixing induced by tidal

25   forcing could either promote NPP by counteracting nutrient depletion or hinder NPP by deteriorating the light environment because of the resuspension and mixing of suspended matter into the euphotic zone.

Key words: North Sea, tides, mixing-stratification, net primary production

1 Introduction

30 Coastal and shelf seas, such as the North Sea, generally show primary production up to 3-5 times that of the open ocean (Simpson and Sharples, 2012). Among the potential reasons for this difference are the tides, one of the dominant physical forcing factors in the North Sea, which regulate the mixing-stratification status (Pingree and Griffiths, 1978; Simpson and Souza, 1995), with potential implications for primary production (Daly and Smith, 1993; Otto et al., 1990). The relevance of tides to primary production has been investigated in a number of previous studies, which show substantial co-variability

35 between hydrodynamic tidal characteristics and biogeochemical data (Blauw et al., 2012; Jago et al., 2002; McCandliss et al., 2002; Pietrzak et al., 2011; Richardson et al., 2000). Tides influence biogeochemical cycling in various ways, enhancing the vertical mixing of biomass, suspended matter and nutrients and causing sediment resuspension. Vertical mixing injects nutrients (e.g., Hu et al., 2008) into the euphotic zone and thereby sustains primary production. However, vertical mixing also promotes the dilution of phytoplankton biomass (Cloern, 1991), which hinders plankton production. The resuspension

40 and upward vertical mixing of near-bottom sediments (Bowers et al., 1998; Smith and Jones, 2015) deteriorate light conditions (Porter et al., 2010) and result in decreasing productivity. The co-action of these mechanisms results in either favourable or unfavourable impacts on ecosystem productivity depending on local hydrodynamic and biochemical conditions, thus shaping the specific structure and sensitivity of North Sea net primary production (NPP).

In the North Sea, several sub-systems emerge with respect to tidal forcing and bathymetry, leading to a high spatial diversity

45 of primary production dynamics (Van Leeuwen et al., 2015) and potentially also NPP sensitivity to tides. In principle, the system can be differentiated into a permanently mixed shallow area in the southern North Sea, a seasonally stratified area in the central and northern North Sea and a transition zone that includes frontal and weakly stratified areas (Schrum et al., 2003). In permanently mixed shallow areas, strong vertical stirring slows the development of the spring bloom and prevents summer nutrient limitation (Wafar et al., 1983). Nutrient availability in shallow coastal areas is additionally enhanced by

50 onshore nutrient and organic matter transport driven by estuarine-type baroclinic circulation (Hofmeister et al., 2017; Rodhe et al., 2004) and land-borne nutrient supplies. Consequently, light limitation is dominant in shallow coastal areas (Tett and Walne, 1995). In contrast, the central and deeper parts of the northern North Sea are seasonally stratified (Pohlmann, 1996), and summer nutrient depletion occurs in the upper mixed layer after the spring bloom (Longhurst, 2006). Because the bottom mixed and surface mixed layers in these regions are largely decoupled, the tidally driven nutrient replenishment from the

55 deeper layers is expected to be rather small. In shallower areas, the bottom mixed layer is able to interfere with the thermocline, and nutrients can be mixed into the euphotic zone (e.g., Rippeth et al. 2008; Richardson et al. 2000, Sharples 2008, Daewel and Schrum, 2013) and sustain the NPP in the euphotic zone in summer. In these areas, the breaking up of stratification is mainly driven by the spring-neap tidal cycle or wind mixing (Mahadevan et al., 2010; Schrum, 1997). The physical mechanisms of the spring-neap cycle, such as the shifting of fronts (Simpson and Bowers, 1981), periodical erosion

60 of the thermocline and relevant ecological responses (Allen et al., 2004), mainly in regard to replenishment of nutrients (Franks and Chen, 1996) and interruption of biomass building (Balch, 1981; Sharples et al., 2006), have been studied

previously. In addition to large-scale stratification patterns that regulate tidal impacts on NPP, local impacts have been observed. The patchiness of chlorophyll (CHL) concentrations at the eastern British coast, for example, was shown to be associated with local vertical mixing generated by tides and bathymetry (Scott et al., 2010). In the Rhine river plume area,

65 suspended particulate matter concentrations are characterized by a periodicity following a fortnight cycle (Pietrzak et al., 2011)

So far, earlier studies have focused largely on the local effects of nutrient injection into the euphotic zone. Understanding key processes and assessing regionally differing responses have been accomplished by cross-frontal field studies and idealized model simulations. (e.g., Cloern, 1991; Richardson et al., 2000; Sharples, 2008). Some of these studies have

70 quantitatively evaluated tidal contributions to NPP based on nutrient replenishment from observed data or 1D simulations using simplified upscaling, neglecting the spatial diversity of the North Sea system. However, it remains an open question how dynamic zooplankton and tide-modulated benthic-pelagic coupling affect the sensitivity of plankton production to tidal forcing. Furthermore, a comprehensive understanding of tidal impacts at a basin scale is still lacking for the North Sea. To answer these questions and investigate highly dynamic tidal impacts on ecosystem productivity in different sub-systems in

75 the North Sea, the application of 3D modelling is indispensable. Here, we will address the above questions using ECOSMO (Daewel and Schrum, 2013; Schrum et al., 2006), a well-validated 3D-coupled physical-biogeochemical model for scenario simulations to elaborate the relevance of tidal impacts on NPP and underlying processes. The model resolves key physical and biogeochemical processes, such as turbulent mixing, zooplankton growth and predation, and impacts of particulate and dissolved organic matter on light conditions. The model has a bottom component, which is dynamically coupled to the water

80 column through the fluxes of particulate and dissolved matter, allowing for resuspension. We will assess the spatial variability of the responses of NPP to major tidal components, i.e., M_2 and S_2, and disentangle different processes contributing to tidally induced variations in NPP, mainly variations related to stratification-mixing patterns, spring bloom onset time and intensity, and the maintenance of NPP in the subsurface of stratified areas. We will further investigate variations in NPP related to the spring-neap tidal cycle.

85 ## 2 Methods

2.1 Model description and validation

In this study, we employed the well-validated 3D-coupled physical-biochemical model ECOSMO (Daewel and Schrum, 2013). The hydrodynamic component of ECOSMO builds on the 3D baroclinic model HAMSOM (HAMburg Shelf Ocean Model) (Schrum and Backhaus, 1999). The capability to simulate the hydrodynamic status of the North Sea-Baltic Sea

90 system was validated by Janssen et al. (2001) and Schrum et al. (2003). The simulation domain covers the North Sea and Baltic Sea, with open boundaries to the northern Atlantic Ocean in the north and the mouth of the English Channel in the south (Fig. 1). The model was formulated on a staggered Arakawa-C grid, which has a spatial resolution of 6'x10'. The model time step was 20 min, which allows for a robust representation of the tidal cycle for physics and biogeochemistry, and

was coupled online using the same time steps as those for hydrodynamics. In this study, we focused on the North Sea region

95   between 5°W–9.5°E and 48°N-58.5°N because tides are only of minor relevance in the Baltic Sea. To resolve thermal

stratification in the upper water column, the vertical resolution was set to 5 m in the upper 40 m of the water column and

decreased gradually with depth below 40 m. To reduce numerical diffusion in the implemented upwind advection scheme, a

shape-preserving total variation diminishing (TVD) scheme (Yee et al., 1985) was adopted, which significantly improved the

representation of hydrodynamics and ecosystem processes, especially processes related to fronts. A detailed description of

100   the method and model responses to the changed advection scheme has been provided by Barthel et al. (2012).

The biogeochemical component of ECOSMO was developed to describe the lower trophic level dynamics of the marine

ecosystem using a N(utrient)P(hytoplankton)Z(ooplankton)D(etritus) conceptual model framework. The ecosystem model

component was first introduced for the North Sea by Schrum et al. (2006a) and further developed for a wider range of

ecosystems, including relevant characteristics for the Baltic Sea, by Daewel and Schrum (2013). Detailed validations against

105   nutrient observations have shown that the model is capable of simulating lower trophic level ecosystem dynamics in the

North Sea, and the temporal variability at inter-annual to decadal scales simulated by ECOSMO could be corroborated by

observations (Daewel and Schrum, 2013). ECOSMO simulates the nutrient cycling of silicate, phosphorus and nitrogen in

the water column and in the sediments considering processes such as primary production, grazing and excretion by

zooplankton, remineralization and sediment-water coupling. A detailed description of the ecosystem model is given in

110   Daewel and Schrum (2013). In total, 16 state variables were solved, including three functional groups for primary producers

(diatoms, flagellates and cyanobacteria). In the second trophic level, two groups of zooplankton were considered and

differentiated based on feeding preferences. To capture the productive and turbid characteristics, dissolved organic matter

(DOM) was parameterized by fast remineralization rates and a low sinking velocity, in contrast to the fast sinking velocity

and slow remineralization rates of particulate organic matter (detritus). To additionally account for the shading effects of

115   DOM and detritus, which were not considered in Daewel and Schrum (2013), the formulation of light attenuation was

amplified as previously suggested by Nissen (2014). Therefore, the vertical light attenuation consisted of background

attenuation (k_{w1}) (induced by water body), phytoplankton self-shading (k_p), and additional shading impacts of DOM (k_{DOM})

and detritus (k_{Det}).

120    $$K1 = k_{w1} + k_p \cdot P + k_{DOM} \cdot DOM + k_{Det} \cdot Det \tag{1}$$

While background attenuation k_{w1} (0.03 m^{-1}, Urtizberea et al., 2013) remained constant in the water column, self-shading

depended on both k_p (0.2 $m^2\ mmolC^{-1}$) and the phytoplankton concentration (P). As suggested by Stedmon et al. (2000)

and Tian et al. (2009), k_{DOM} and detritus k_{Det} were set to 0.29 $m^2 gC^{-1}$ and 0.2 $m^2\ gC^{-1}$, respectively. Compared to

125   Daewel and Schrum (2013), these changes enabled the dynamical coupling of turbidity to the seasonal production cycle, as

previously discussed by Nissen (2014). The model was thereby capable of resolving tidal influences on primary production

via potentially competing processes. Tidal mixing releases nutrient limitation, thus fostering NPP, but tides also cause the resuspension and mixing of suspended matter into the euphotic zone, which reduces light availability in the water column, thus reducing NPP. In addition to relevant bottom-up processes, the model also resolved predator–prey interactions and

130   vertical oxygen and temperature profiles, which alter the remineralization of organic matter and consequently nutrient cycling.

The ability to properly resolve intensified frontal production and the consideration of key processes influencing light and nutrient limitation related to tidal forcing make ECOSMO an appropriate tool to assess tidal impacts on NPP in the spatially highly diverse North Sea. As already stated in Daewel and Schrum (2013), ECOSMO estimates of annual NPP in the North

135   Sea (Fig. 2b) are at the lower edge of what has been simulated for the area (Holt et al., 2012; van Leeuwen et al., 2013). The relatively low estimates mainly appear in the northern North Sea (NNS), where primary production is estimated to be approximately 125 $gCm^{-2}y^{-1}$ based on observations (Van Beusekom and Diel-Christiansen, 1994), and in the southern coast, where NPP observations range between 199-261 $gCm^{-2}y^{-1}$ (Joint and Pomroy, 1993). The simulation fits well with observation-based estimates of NPP in the British coast of approximately 75-79 $gCm^{-2}y^{-1}$ (Joint and Pomroy, 1992) and

140   primary production estimates of 100 $gCm^{-2}y^{-1}$ and 119-147 $gCm^{-2}y^{-1}$ in the central parts of the North Sea and at Dogger Bank, respectively (Joint and Pomroy, 1993).

2.2 Model setup

A detailed description of the model setup was given by Daewel and Schrum (2013); therefore, we will only provide a brief overview of the forcing data used for the model simulation, particularly emphasizing the changes made to the previously

145   described setup. These changes mainly concern the river discharge and nutrient load data sources. The simulation was initialized in 1948 using climatological data from the World Ocean Atlas (WOA) (Conkright et al., 2002) for nutrients and observational climatology for temperature and salinity (Janssen et al., 1999). The full simulation period encompasses 68 years, ending in 2015, and is forced with atmospheric boundary conditions provided by the NCEP/NCAR reanalysis (Kalnay et al., 1996). Additional forcing data include wet deposition for nitrogen, which were prescribed using data from a

150   Community Multiscale Air Quality (CMAQ) model (Matthias et al., 2008), and boundary values for nutrients, temperature and salinity at the open boundaries to the North Atlantic, for which we used the same climatological data as those used for the initial conditions. For salinity, additional annual anomalies were retrieved from observational data available at the ICES (International Council for the Exploration of the Sea) database (http://www.ices.dk). An updated set of river runoff and nutrient load data was applied with more complete river forcing data coverage for the North Sea and Baltic Sea. A multitude

155   of data were provided by Sonja van Leeuwen (Royal Netherlands Institute for Sea Research , pers. communication) containing the following datasets: UK data were processed from raw data from the Environment Agency (England and Wales, contains Natural Resources Wales information © Natural Resources Wales and database rights), the Scottish Environment Protection Agency (Scotland), the Rivers Agency (Northern Ireland) and the National River Flow Archive. French water quality data were provided by Agence de l'eau Loire-Bretagne, Agence de l'eau Seine-Normandie, OSUR web

160   Loire-Bretagne and SIEAG (Systeme d'information sur l'eau du bassin Adour Garonne), while daily flow data were obtained from Le Banque Hydro (www.hydro.eaufrance.fr). German and Dutch riverine data were provided by the University of Hamburg (Pätsch, J., Lenhart, 2004). Norwegian water quality data were provided by the Norwegian Water Resources and Energy Directorate (NVE), with daily flow data supplied by the Norwegian Institute for Water Research (NIVA). Danish water quality data were provided by the National Environmental Research Institute (NERI). Water quality data for Baltic

165   rivers were provided by the University of Stockholm and the Baltic Nest. Furthermore, nutrient status and freshwater runoff information in the southern and eastern Baltic Sea was supplemented by data from the Balt-Hype model (Arheimer et al., 2012; Lindström et al., 2010). Nutrient loads from Danish waters were provided by Marie Maar (pers. communication) and were similar to the forcing data used for the HBM-ERGOM simulation (Maar et al., 2016). These data stem from a national monitoring program (Windolf et al., 2011, 2012) and from the hydrological Denmark model, which provides runoff

170   calculations for ungauged areas of Denmark (Henriksen et al., 2003).

We selected a relatively short time period (1990-2015) for our analysis to assure a long enough spin-up time that accounts for the characteristic long time scales of the North Sea-Baltic Sea system (Daewel and Schrum, 2013). The period from 1990-2015 will hereafter be called the *analysed period*. Tidal cycles with long periods, such as the nodal and elliptical cycles, although considered in the forcing via nodal corrections of partial tide amplitudes and phases (see 2.3), are not

175   targeted in this study.

2.3 Tidal forcing and scenarios

Sea surface elevation was prescribed at the open boundaries, with a time step of 20 min. Daily mean sea surface elevation data were taken from a diagnostic model simulation for the wider northeast European Shelf (Backhaus and Hainbucher, 1987) and also forced with the NCEP/NCAR reanalysis. In addition, tidal elevations were calculated from tidal constituents

180   provided by the German Federal Maritime and Hydrographic Agency (Federal Maritime and Hydrographic Agency Deutsches Hydrographisches Insititut, 1967) . Nodal corrections were implemented in the calculation of tides to represent the long-term variation in lunar nodes. For the standard tidal scenario, partial M_2 tide (principle lunar tide) and S_2 tide (principle solar tide) (Thomson and Emery, 2014) were considered; we hereafter call this scenario the *tidal scenario*. To evaluate the contribution of the spring-neap tidal cycle, a tidal scenario using only the M_2 partial tide, called the *M_2 scenario,* was

185   simulated and discussed in comparison to the *tidal scenario*. To quantify the overall impact of tidal forcing, a scenario without tidal forcing at the open boundary was simulated to yield the non-tidal reference state of the system (*non-tidal scenario*).

2.4 Postprocessing of model results

The responses of ecosystem productivity to tidal forcing were assessed by comparing the annual mean NPP during the

190   *analysed period* between the *tidal* and *non-tidal scenarios* (*tidal scenario* minus *non-tidal scenario*). Furthermore, we disentangled processes that might contribute to variations in NPP, such as the seasonality of spatial patterns in limitation

Earth System
Dynamics
Discussions

factors (nutrients vs. light), spring bloom phenology, the impacts of the spring-neap cycle on NPP variability, and the contribution of subsurface production to the overall NPP. We quantified these processes using subdomains and further made comparisons between scenarios, emphasizing spatial variability and the seasonal cycle.

2.4.1 Process-based subdomain division

The pre-division of the area into subdomains was based on a combination of the local responses of NPP to tidal forcing (increase, decrease), bathymetry and geographic locations. Based on these criteria, the southern North Sea (SNS) was divided into three subdomains based on the response patterns of NPP to tidal forcing (Fig. 2). In principle, the SNS can be separated into an area responding with increased NPP (*pos. SNS*) and decreased NPP (*neg. SNS*) to tidal forcing. The English Channel (EC) was treated differently because of the strong tidal currents in this area compared to the rest of the SNS. The identification of the EC was based on geographical location and included the area south of 52°N. The NNS and SNS were divided by the 65 m isobath. The Norwegian Trench (NT) was characterized by a water depth deeper than 200 m. Apart from the NT, the region of the NNS was further divided based on the magnitude of the response of NPP to tidal forcing. Based on this pre-division of subdomains, we identified the most representative grid cell within each subdomain using correlation analysis (Eliasen et al. 2017, Appendix A). To identify the most representative grid cell location in each subdomain, we first produced a time series of the NPP differences between the *non-tidal scenario* and *tidal scenario* for each grid cell. Subsequently, we estimated, for each of the grid cells, the correlation to the time series of the other grid cells within the same pre-divided subdomain. The grid cell with the highest correlation coefficient to all other grid cells in each subdomain was selected as the most representative point for further analysis.

2.4.2. Quantification of key processes controlling the spring bloom

The peak amplitude and the onset time of the spring bloom for the different scenarios were compared. The onset of the spring bloom is defined here as the day when the daily vertically integrated NPP reaches its maximum prior to the spring maximum in diatom biomass (Appendix B), as used in Sharples et al.'s study (Sharples et al., 2006). Diatom time series were pre-processed by a 15-day running mean to remove short-term maxima induced by the spring-neap tidal cycle (Sharples et al., 2006). To further disentangle mechanisms resulting in spring bloom phenology differences among the scenarios, we quantified potentially related biological and physical factors relevant for spring bloom dynamics, such as the zooplankton biomass prior to the onset of the spring bloom, light conditions and development of stratification, for each grid cell.

In particular i) the vertically averaged zooplankton biomass in the winter season (January/February) was considered a proxy for potential grazing pressure at the beginning of the growth season. ii) The integrated value of the light-limiting term in the upper 50 metres of the water column was used to estimate the light conditions for phytoplankton growth. To quantify the time when the light was sufficient for phytoplankton growth in each year, we estimated the date when the integrated light limiting term exceeded 0.85 for three consecutive days. iii) The onset of stratification was quantified by recording the time

when the maximum vertical temperature difference in the water column exceeded 0.5°C for three consecutive days. A time

225 window (3 days) was chosen to filter out short-lived stratification variations and the day-night heating/cooling cycle. iv) The

averaged mixed layer depth in May was used as a measure for stratification depth.

Applying the methods mentioned above, we identified the onset time of the spring bloom, the time for the establishment of

stratification and the time when light conditions were sufficient for phytoplankton growth, as well as the biomass levels of

phytoplankton and zooplankton in the analysed period. For each simulation year, the time identifiers were recorded in days

230 of the year, which enabled the quantification of the number of years when the time identifier was postponed or advanced by

tidal forcing (e.g., if in 13 of 26 *analysed period* years, the onset time of the spring bloom was delayed, the delayed

percentage was 50% at the particular location). This enabled a direct comparison of the resulting spatial patterns. In total, we

obtained the percentage of years after applying the tidal forcing with a 1) higher amplitude of the spring bloom, 2) later onset

of the spring bloom, 3) later onset of stratification, 4) deeper mixed layer depth, 5) later occurrence of sufficient light

235 conditions for building phytoplankton biomass, and 6) higher concentration of winter zooplankton in the *tidal scenario* than

in the *non-tidal scenario*.

Additionally, we associated changes in the spring bloom phenology to the spring-neap tidal cycle. Considering that several

spring-neap cycles may take place during the spring bloom development, we set the NPP difference between the two

scenarios (*tidal scenario & M₂ scenario*) in relation to the spring-neap tidal phase. The period of spring bloom development

240 was defined as the time period with an increase in NPP from 12.5% to 87.5% of the maximum NPP. During this time period,

we identified the occurrences (within a time window of one fortnight cycle) of positive/negative maxima of the NPP

difference and the temporal relation of these occurrences to the adjacent day of the spring tide. This enabled us to evaluate

the impact of spring-neap tidal cycles on spring bloom phenology.

2.4.3 Quantification of limiting pattern of phytoplankton growth: light vs. nutrients

245 In ECOSMO, NPP is estimated as the sum of net primary production for all phytoplankton functional groups (Eq.2, denoted

by j). For each functional group, the net primary production (NPP) is calculated by multiplying the maximum growth rate

specified for the functional group (σ_j) with the minimum value (φ_j) of all limiting terms (θ) (Liebig's law, de Baar, 1994)

and the prevailing amount of phytoplankton biomass (standing stock, C_j) (Eq. 2). The limiting term (θ) for each growth

resource is derived from the Monod equation (Monod, 1942), using the concentration of each growth resource(β) (Si:

250 silicate-only for diatom growth, N: nitrogen, P: phosphorus, L: light) and the specific half-saturation constant (h) (Eq. 3).

Further details of the nutrient limiting terms are given in Daewel and Schrum (2013). We hereafter call the minimum value

of all limiting terms φ (Eq.4) the limiting value. The limiting value quantifies the availability of growth resources with a

range of 0-1. The closer the value is to 1, the more sufficient the resource is. Additionally, we identified the most limiting

factors for each phytoplankton type (φ_j) (N, P, and L for flagellates; Si, N, P, and L for diatoms).

255

Earth System
Dynamics
Discussions

$$NPP = \sum_{j=1}^{3} \sigma_j \varphi_j C_j \tag{2}$$

$$\theta = \beta / (\beta + h) \tag{3}$$

$$\varphi = min(\theta_{light}, \theta_N, \theta_P, \theta_{Si}) \tag{4}$$

260 We analysed the limiting value to represent the environmental conditions of phytoplankton growth and the spatial and temporal dynamics of the most limiting factor.

2.4.4. Vertical distribution of phytoplankton: detection of subsurface maximum layer

The mixing intensity in the water column controls the distribution of phytoplankton and nutrients. As suggested by previous studies, phytoplankton may develop high subsurface concentrations in layers of low turbulence such as the pycnocline;

265 production continues locally in low-turbulent zones as long as the growth requirements of nutrients and light are balanced (Cullen, 2015). In the stratified season, we differentiated the NPP generated in the surface layer (above 15 m) and in the subsurface layers, as a subsurface biomass maximum (SBM) emerged. The SBM was defined by its width, which was small compared to the water depth, and was persistent in both time and space (Dekshenieks et al., 2001). In this study, we regarded layers deeper than 15 m as the subsurface. As an SBM necessarily includes local peaks, we first selected the depth at which

270 the first-order derivative of biomass changed from positive to negative in the vertical biomass profile as a potential location for an SBM peak. To further identify the boundaries of the potential SBM, different strategies were applied depending on the number of vertical layers on either side of the potential SBM peak. If there were more than 5 vertical layers on either side of the potential SBM peak, the vertical layer with the local maximum in the second-order derivative on each side of the potential SBM peak was recognized as the boundary of the SBM layer (Benoit-Bird et al., 2009). Otherwise, the adjacent

275 layers were assumed to confine the potential SBM. The SBM peak could be no shallower than 20 m. We estimated the local background biomass value by linearly interpolating the biomass values of the upper and lower edges to the depth where the peak in biomass emerged. If the peak maximum biomass exceeded 1.5 times higher than the estimated background biomass in the respective water column, the local vertical plankton biomass maximum was considered an SBM.

2.4.5 Identification of representative points for spring-neap cycle impacts

280 Although driven by astronomical forcing, the energy of tidal currents interacts with atmospheric forcing (Davies and Lawrence, 1994; Jacob and Stanev, 2017). Furthermore, non-linear interactions among tidal constituents are pronounced in shallower waters, as suggested by Backhaus (1985) in inshore areas for the German Bight and Danish Coast. Although we preliminarily estimated the influence of the spring-neap tidal cycle via the difference in NPP between the *tidal scenario* and the *M₂ scenario*, related responses would not necessarily be visible in a fortnightly cycle. To better associate the variation in

285 NPP with the spring-neap tidal cycle, we identified specific grid cells where both currents and biochemical factors displayed a distinguishable spring-neap cycle. Those locations were identified by using the estimated squared coherence between the

Earth System
Dynamics
Discussions

power spectra (SCPS) of currents and NPP (Stoica et al., 2005; Welch, 1967). By adopting the SCPS method, we were able to select representative grid cells where both NPP and velocity showed obvious spring-neap cycles.

3. Results & Discussion

290   3.1 Spatial changes in mean production

The average annual NPP and the difference in NPP between the *tidal* and *non-tidal scenarios* are shown in Fig. 2. The area-averaged NPP increases slightly from 100.7 to 103.2 $gCm^{-2}y^{-1}$ when tidal forcing is applied (Table 1); however, high spatial diversity in the sensitivity to tidal forcing is shown. Generally, estimated tidal impacts on NPP are highest in the stratified shallow North Sea, with a maximum response of up to 60 $gCm^{-2}y^{-1}$ (Fig. 2c). In the *non-tidal scenario*, high

295   productivity is restricted to the near-shore shallow regions along the British coast and the European continental coast (Fig. 2a), which are the main regions where the euphotic zone reaches the bottom and nutrient remineralization fosters production throughout the year. The primary production at the coast is additionally supported by estuarine-type baroclinic circulation in summer, which transports detritus and nutrient-rich bottom water towards the coast (Ebenhöh et al., 2004; Geyer and MacCready, 2014; Hofmeister et al., 2017). Tides cause a significant reduction in stratification in the shallow near-coastal

300   areas of the North Sea and in the EC at Dogger Bank and south of Dogger Bank and foster the development of tidal mixing fronts. Consequently, the production pattern changes notably when tidal forcing is considered. The primary production maximum is shifted further offshore towards the frontal region (Fig. 2b). Large areas of the SNS, including Dogger Bank, the eastern BC, and the Danish Coast in the east, together with the NT, exhibit an increase in NPP when tidal forcing is prescribed. The shallow near-coastal areas in the south and the deeper areas in the NNS show a negative response of NPP to

305   tidal forcing. A stronger negative response is observed in the highly dynamic EC (Fig. 2c). The NPP of Dogger Bank and the tidal mixing front area south and southeast of Dogger Bank responds the strongest to tidal forcing, with a mean change in NPP of up to 60 $gCm^{-2}y^{-1}$, nearly doubling local production. The amplitudes of the decreases in NPP in the negatively responding area are smaller than those of the increases in NPP, with amplitudes no more than 40 $gCm^{-2}y^{-1}$ (Fig. 2c); the largest amplitudes are in the EC.

310   The tidally induced change in NPP is associated with variations in the spatial distribution of the main limiting resources (limiting pattern) (Fig. 3). Generally, in the *tidal scenario*, the area experiencing nutrient limitation decreases due to the enhanced mixing of inorganic nutrients into the euphotic zone, especially in the shallow North Sea where the bottom and surface mixed layer interact with each other. Simultaneously, light limitation increases. The predominantly light-limited regions, which are restricted to the shallow coastal regions in the *non-tidal scenario* (Fig. 3a), expand offshore in the tidal

315   scenario (Fig. 3b). Tidally induced resuspension and mixing of particulates and DOM into the euphotic zone result in dominant light limitation in almost the entire shallow North Sea (below 50 m depth) (Fig. 3b). In contrast, in the surface layers of the stratified area, summer nutrient limitation is predominant, and the limiting value remains below 0.3 in both

scenarios. The change from nutrient to light limitation in the SNS changes the limiting value to >0.4 in the *tidal scenario,* allowing better resource exploitation in these areas and sustaining NPP during summer.

320 The subdomain-division method described in section 2.4.1 identifies 7 different subdomains (Fig. 4) that show characteristic responses to tidal forcing. Based on the division and the point-wise correlation of NPP variations in each subdomain (appendix A), representative grid cells were selected to study the mechanisms underlying the spatial variability of tidal responses in detail. Areas with correlation coefficients higher than 0.3 occupied at least 53% of each subdomain, comprising 77% of the entire study area. This indicates that the division effectively explains the spatial diversity of the system with

325 respect to the tidally induced changes in NPP and the predominantly inherent similarity within each subdomain. The seven identified subdomains are listed below (Fig. 4):

1. *The English Channel (EC; dark blue)* is characterized by an early onset of the spring bloom, strong mixing due to tidal stirring and shallow bathymetry. The *EC* is the most productive area in the *non-tidal scenario* (Fig. 2a), with a mean NPP above 120 $gCm^{-2}y^{-1}$.

330 2. *Negatively responding southern North Sea (neg. SNS; blue).* The *neg. SNS* is separated from the EC by 52°N and from the positively responding area in the southern North Sea. The *neg. SNS* characterizes the permanently mixed area in the shallow water near the coast.

3. *Positively responding southern North Sea (pos. SNS; light blue).* This area includes the frontal regions that were identified as the areas with the highest responses in NPP (Fig. 2).

335 4. *Eastern British coast (BC; green).* This area is a highly productive, positively responding inshore region of the eastern British coast.

5. *Deeper northern North Sea (deep NNS; yellow).* The *deep NNS* region coincides with areas of seasonal stratification and the lowest annual NPP in the *tidal scenario* (Fig. 2). In this area, a slight decrease in NPP is estimated when tidal forcing is considered.

340 6. *The Norwegian Trench (NT; orange)* represents the area off the Norwegian coast, which is strongly impacted by the low saline outflow from the Baltic Sea. The *NT* shows a slight increase in NPP due to tidal forcing (Fig. 2).

7. *Low-sensitivity area in the northern North Sea (low-sen. NNS).* The magnitude of the response of NPP to tidal forcing here is below 5 $gCm^{-2}y^{-1}$. This subdomain is influenced by two amphidromic points in the eastern North Sea, with tidal amplitudes of the M$_2$ partial tide generally below 0.5 m.

345 Some narrow transient zones between the positively responding areas and negatively responding areas are shown in white in Fig. 4. These transient zones with an absolute variation in NPP less than 5 $gCm^{-2}y^{-1}$ are excluded from the following analyses. Changes in NPP in response to tidal forcing for each subdomain are listed in Table 1.

The subdomain division corresponds well with the regional characteristics of M$_2$ tidal energy dissipation rates, as suggested by the simulation study of Davies and Sauvel (1985). The *EC* subdomain includes the areas with the highest tidal energy

350 dissipation rates, which exceed 1000 $Jcm^{-2}s^{-1}$ (Davies and Sauvel, 1985). In most of the *neg. SNS* and some parts of the *EC*, the tidal energy dissipation rates are in the range of 100-1000 $Jcm^{-2}s^{-1}$. In the *pos. SNS*, the *BC* and part of the *deep*

NS, tidal energy dissipation rates range from 10 to 100 $Jcm^{-2}s^{-1}$. The *low-sen. NNS* and *NT* are located in the area with tidal energy dissipation rates below 10 $Jcm^{-2}s^{-1}$. The strong tidal energy in the SNS destabilizes stratification, as also revealed by the subdivision based on stratification patterns presented by Van Leeuwen et al. (2015). Our *neg. SNS* and *EC*

355 subdomains coincide with permanently mixed regions defined in the above study; in addition, the defined *BC* correlates with mixed or temporally stratified belts along the eastern British coast, as suggested by Van Leeuwen et al. (2015). The subdomains identified in the NNS coincide with seasonally stratified areas in the aforementioned study. However, the majority of *pos. SNS,* which shows the strongest response to tidal forcing, could not be identified with the method of Van Leeuwen et al. (Van Leeuwen et al., 2015). due to the variable stratification in these frontal areas induced by the spring-neap

360 cycle, wind forcing, river runoff and air temperature (Dippner, 1993; Schrum et al., 2003; Sharples and Simpson, 1993). The subdomains also agree well with subdomains previously identified by ICES (ICES, 1983). Compared to the ICES subdivisions, which were determined considering biochemical and hydrographical characteristics (ICES, 1983), the northern 4 subdomains in our study coincide with regions where the gross water mass influx is mainly influenced by Atlantic water inflow. In contrast, for the 3 subdomains in the south, the influence of wind is more important for water mass exchange

365 (Siegismund, 2001).

3.2 Characteristic seasonal changes

Out of the 7 subdomains (Fig. 4), we selected 3 representative subdomains for further analysis of the changes in seasonality of NPP and the respective associated mechanisms. The *neg. SNS* represents the southern coastal area where strong tidal forcing leads to permanent mixing and the NPP decreases as a consequence of tidal forcing. The *pos. SNS* embodies the

370 transient zone between mixed and stratified water column and is characterized by the most significant positive response of NPP to tidal forcing. The *deep NNS* is characterized by stable seasonal stratification. Here, the bottom mixed layer and surface mixed layer are well separated; thus, tides have a limited impact on the euphotic zone. The averaged time series (1990-2015) for each subdomain and the time series of the vertical profiles of each most representative grid cell (see section 2.4.1) are given in Fig. 5 and Fig. 6, respectively.

375 In the *neg. SNS* (Fig. 5a), the spring bloom is delayed and strong fluctuations appear during the productive season in both scenarios (Fig. 5a & Fig. 6 a, b, c, d). The pulses in NPP are probably due to predator-prey interactions and possibly modulated by advection. These pulses in NPP have previously been described by (Tett and Walne, 1995). The length of these fluctuations is slightly longer in the *tidal scenario* than in the *non-tidal scenario*, and changes in bloom initiation and the length of the quasi-periodic fluctuations generate positive-negative fluctuations in the NPP difference between both

380 scenarios. We found no nutrient limitation in the water column in either scenario (Fig. 6 a, b) and no significant changes in the limiting values (Eq. 4) (note: the minimum limiting value stems from light limitation), except for the slightly higher values in deep water column under the *tidal scenario* (Fig 6. c, d). This exception is likely caused by the downward mixing of shade-producing organic materials (e.g., phytoplankton, DOM and detritus), which leads to improved light conditions in the upper layer and better penetration. However, this result does not explain the negative NPP response in the area. Lower

385   NPP in the *tidal scenario* than in the *non-tidal scenario*, especially in spring and early summer, results in an overall negative response in NPP. A likely reason for the reduction in NPP in the *neg. SNS* subdomain could be the tidally induced dilution of phytoplankton biomass in the euphotic zone in the shallow areas. The increased mixing in the *tidal scenario* dilutes the phytoplankton concentration in the upper, highly productive water layer and consequently reduces the time during which phytoplankton cells are exposed to high surface irradiance. Grazing pressure could be rejected as the major cause for the

390   decreased NPP because grazing pressure is also higher under more productive conditions (data not shown). Considering the small difference in the growth resources between the two scenarios (Fig. 6 c, d), we mainly attribute the variation in NPP to the vertical distribution of standing stocks.

The most dominant change in seasonality as a consequence of tidal forcing in the seasonally stratified subdomains (*pos. SNS* and *deep NNS*) is the delay of the spring bloom in the *tidal scenario* (Fig. 5b, c). However, in the *pos. SNS*, this delay is only

395   a few days long; in the *deep NNS*, this delay encompasses one month. Accompanying the delay, the amplitude of the spring bloom in the *tidal scenario*, especially in the *pos. SNS*, exceeds that of the *non-tidal scenario*. The spring bloom in the NS typically consists of diatoms, while after silicate depletion, flagellates dominate the summer production (McQuatters-Gollop et al., 2007; Schrum et al., 2006). Comparing the seasonality of NPP variation (Fig. 5b, c) with the annual averaged NPP deviation between scenarios (Fig. 2c), we found that the variation in NPP in summer is basically in phase with the direction

400   of the NPP's response to tidal forcing for both the *deep NNS* and *pos. SNS*. Especially in the *pos. SNS* (Fig. 5b), summer blooms are higher in the *tidal scenario* than in the *non-tidal scenario*, with a maximum difference in July and August, fostered by weaker stratification and regular nutrient injections into the surface mixed layer due to tidally induced turbulence (Fig. 6f, h). Surface summer production is sustained throughout the summer at values of approximately 50 $mgCm^{-3}d^{-1}$ and more in the upper 15 m (Fig. 6f), and light remains the dominant limiting factor in the surface layer, except for a temporal

405   silicate limitation after the spring bloom (Fig. 6 h). In contrast, without tidal stirring, surface waters become nutrient depleted soon after the spring bloom in May. After silicate limitation, nitrogen limitation persists (Fig. 6 g) in the surface waters throughout theseasonal stratification, which results in the characteristic subsurface production in summer (Fig. 6e). Due to the weaker stratification and enhanced turbidity caused by tides, no SBM production occurs in this simulation. The nutrient supply advantage in the *tidal scenario* persists until the beginning of October (Fig. 6f), when the water column in the *non-*

410   *tidal scenario* is also mixed by atmospheric conditions, causing an increase in production at the surface.

In the *deep NNS*, the influence of tides on NPP is relatively weak and mainly visible in summer (Fig. 5c). The *deep NNS* (Fig. 6i-l) is typically characterized by stable seasonal stratification and summer subsurface primary production in both the *tidal* and *non-tidal scenarios*. The delay of the spring bloom in the *tidal scenario* causes a quicker succession and consequently overlapping diatom and flagellate blooms (Fig. 6l, Fig. 5c). The productive period, which lasts nearly 3 months

415   and includes two pulses of NPP in the *non-tidal scenario* (Fig. 6i), is shortened to 6 weeks in the *tidal scenario* (Fig. 6j). The NPP contributed from subsurface production is higher in the *tidal scenario* than that in the *non-tidal scenario* (Fig. 6i, j).

In the other identified subdomains (results not shown), the changes in primary production basically follow the pattern explained above. In the *EC* subdomain, the tidal impact on production is comparable to that in the *neg. SNS*, whereas in the

BC subdomain, nutrients are rarely the most limiting factors due to weak stratification, and the response can be compared to

420   that in the *pos. SNS*. In the *low-sen. NNS,* where tidal dissipation is weak, the vertical distribution pattern of NPP in both

scenarios is almost identical.

Our results indicate that, in principle, tidal stirring causes two major changes in the NPP pattern: i) a change in the spring

bloom phenology of some areas and ii) an altered ratio between surface and subsurface production. Both features merit

further discussion, which is given in the following paragraphs.

425   **3.2.1 Changes in spring bloom phenology**

As one of the most important biological events in the NPP annual cycle (Bagniewski et al., 2011; Sabine et al., 2004), the

spring bloom requires specific attention. As shown by the time series analysis for some subdomains (Fig. 5) and the time

series of profiles at the representative points (Fig. 6), the postponement of the spring bloom is a prevalent phenomenon when

tidal forcing is applied. The changes in spring bloom phenology and the processes responsible for these changes , such as the

430   delay in the onset of stratification, variations in light conditions, the mixed layer depth and winter zooplankton

concentrations (Fig. 7), were analysed using the method outlined in section 2.4.2.

In line with the distribution of tidal energy dissipation given by Davies and Sauvel (1985), the spring bloom delay is robust

in the SNS and along the British coast(Fig. 7a), while in the northeastern part of the North Sea, the spring bloom is delayed

in no more than 50% of all years. An increase in the peak spring bloom biomass (Fig. 7b), mainly in areas with a positive

435   response of NPP to tidal forcing (Fig. 2c). However, in some isolated locations in the negatively responding areas, such as

the *neg. SNS* and *EC*, the spring bloom amplitudes are still higher in the *tidal scenario* than that in the *non-tidal scenario* in

more than 50% of the years. One potential reason for the spring bloom delay is a change in light conditions, especially in

very shallow coastal, non-stratified areas where tidal stirring enhances resuspension in the water column (Fig 7c). The onset

of light conditions sufficient for phytoplankton growth in the well-mixed water column is delayed in the coastal areas of the

440   southern and eastern boundary and in the shallower parts of Dogger Bank. However, the distribution of this impact does not

explain the major patterns of changes in the spring bloom phenology. Tides also increase mixing and hence potentially

prevent stratification in shallow water columns or delay the onset of stratification, as discussed previously by a number of

authors (Bowden and Hamilton, 1975; Loder and Greenberg, 1986). Because tidally induced energy dissipation is cubically

proportional to the strength of tidal currents (Simpson and Hunter, 1974), we can expect the strongest variation in

445   stratification in regions with the strongest tidal currents, as observed along the British coast, in the *EC* and in the German

Bight (Davies and Sauvel, 1985). This expectation is supported by earlier observations suggesting that the onset of the spring

bloom is triggered by improved light conditions because of solar radiation and stratification (van der Woerd et al., 2011).

The onset of stratification (Fig. 7e) in the *tidal scenario* is mainly delayed in the Scottish coast and the frontal areas of the

SNS. Furthermore, the response of stratification to tidal forcing is more stable in the southwestern part (the Estuary of

450   Humber, Dogger Bank) than in the southeastern part of the SNS(Fig. 7e). Apart from solar heating, the stratification in the

southeastern part of SNSis additionally influenced by freshwater supplies from land and wind forcing (Jacobs, 2004;

Ruddick et al., 1995; Schrum, 1997). Consequently, the variation in the onset of stratification is less clear in the southeastern part than in other parts of the SNS. In the NNS, the tidal wave propagation deepens the mixed layer depth (Fig. 7d), which similarly results in a later onset of the spring bloom, despite only weak changes in the onset of stratification. As a

455 consequence of the thicker layer in which phytoplankton are mixed, the phytoplankton are less exposed to the favourable surface light conditions and will thus take longer to build up the spring bloom biomass.

Although the North Sea is in principle a bottom-up-controlled ecosystem, zooplankton predation is occasionally an important process controlling NPP (Daewel et al., 2014). In early spring, even under favourable growth conditions, the spring bloom will only initiate until production exceeds the loss due to grazing (George et al., 2015; Martin, 1965). This grazing pressure

460 is basically correlated with the overwintering zooplankton stock. Based on our results, increases in the winter zooplankton biomass and delays in the spring bloom coincide only in the frontal region of the SNS and central NNS. Therefore, we conclude that the delay in spring bloom by tides is mostly due to bottom-up control.

The spatial pattern given in Fig. 7 shows that the delayed onset of the spring bloom in the *tidal scenario* may mainly be attributed to deteriorated light conditions in the shallow well-mixed area (Fig. 7c) and changes in the stratification of

465 seasonally stratified areas, such as delays in the development of stratification (Fig. 7e) or the deepening of the upper mixed layer (Fig. 7d). Although the predator biomasses are higher prior to spring bloom in some areas, enhanced grazing pressure at the beginning of the bloom period does not seem to be the main mechanism delaying the onset of the spring bloom (Fig. 7f), although we assume this pressure plays an additional role in the central NNS and frontal regions.

3.2.2 Changes in subsurface production in stratified season

470 To further quantify the magnitude of the changes in surface and subsurface production during the stratified season, we separated NPP vertically into upper-layer production (above 15 m) and production in the SBM layer and compared the results between scenarios (Fig. 8), using the mean annual value for the *analysed period* (1990-2015). At the stratified side of the frontal zones (*pos. SNS*), the surface production response of NPP is positive almost everywhere, with a maximum reaching $+50\ gCm^{-2}y^{-1}$ (Fig. 8b) at south of the Dogger Bank. In contrast, the changes in response to tidal forcing within

475 the SBM show both negative and positive responses around the Dogger Bank (Fig. 8a). A positive response to tidal forcing, which is generally one order of magnitude smaller than the increased amplitude of NPP in the surface layer, occurs only at the northern edge around Dogger Bank and the deeper part of the German Bight. A similar pattern with a strong positive response to tidal forcing at the surface and a negative response in the SBM appears in the BC area. In line with former studies in the North Sea, the NPP in the upper layer dominates the whole production budget (van Leeuwen et al., 2013).

480 Although the expansion and duration times of the SBM decrease due to tidal forcing, e.g., in the inshore areas along the BC and at the Danish Coast (Appendix C b, d), tidal forcing promotes NPP within the SBM in some areas, especially at the northern edge of the Dogger Bank. Observational studies suggested that the productive areas at the edge of the Dogger Bank are fueled by baroclinic circulation related to the front and the spring-neap adjustment (Pedersen, 1994). When considering

485   an SBM duration of 110 days (Appendix C c) at the northern edge of the Dogger Bank, the average daily NPP (deduced from the annual NPP (Appendix C, a)) is approximately 239 $mgC\ m^{-2}d^{-1}$, which corroborates the observation-based estimate of NPP (295 $mgC\ m^{-2}d^{-1}$) calculated from measured oxygen surplus concentration data (Richardson et al., 2000).

In the NNS, the variation caused by tidal forcing in NPP is below 15 $gCm^{-2}y^{-1}$ (Fig. 2c). In some parts of the *deep NNS*, the tidal forcing causes higher production in the SBM and lower production at the surface (Fig. 6i, j; Fig. 8a). Due to the

490   decoupling between the surface and bottom mixed layers, the pycnocline acts as a barrier that keeps the stirred-up nutrients below the pycnocline and sustains NPP in the SBM (Fig. 6i, k). Because the amplitude of NPP variations in the upper layers is ten times higher than that in the SBM (Fig. 8), the overall response to tidal forcing is negative (Fig. 2c) in the *deep NNS*.

3.3 Impacts of the spring-neap cycle

The spring-neap tidal cycle introduces a fortnightly periodic change in tidal mixing, which has a significant influence along

495   the British coast and in the English Channel (Fig. 9). The differences in current speed between the *tidal and M₂ tidal scenarios* vary over the spring-neap tidal cycle. The maximum spring-neap range of these differences is up to 0.3-0.6 m/s (Fig. 9), indicating that a non-negligible change in turbulent kinetic energy is introduced to the water column via the spring-neap cycle. Here, we will provide model estimates on the spatial variability in the resulting response of the NPP to the spring-neap cycle and explore the potential mechanisms of these responses.

500   Annual NPP changes induced by the spring-neap cycle reach maximum values of up to 5 $gCm^{-2}y^{-1}$ (Fig. 9). Although this amount is relatively small compared to the overall system productivity, the changes due to spring-neap dynamics could be very relevant locally and in specific time periods. An average positive response of NPP emerges in the southeastern part of the North Sea, in the English Channel and along the British Coast (Fig. 9). The highest mean changes in NPP are found in the western part of the Dogger Bank, in the English Channel and off the Scottish coast. In contrast, a negative response in

505   annual production emerges off the Northumbrian coast and in the Southern Bight off the European continent (Fig. 9). The response of NPP to spring-neap tidal forcing is weak in early spring and winter (data not shown). Under mixed conditions or during periods of the establishment and decay of stratification, spring-neap tidal mixing can be overridden periodically by other mixing events (e.g. driven by wind); hence, pronounced irregularities in NPP responses to spring-neap tidal forcing are detected. A significant response of NPP to spring-neap tidal forcing is found for summer periods under stable stratification.

510   To illustrate the basic mechanisms responsible for the response of NPP due to spring-neap tidal cycle, we present time series of the biomass, nitrate, NPP and turbidity (Eq. 1) profiles for two characteristic grid cells (selection described c.f. 2.4.5) that respond differently to spring-neap tidal forcing. The near-shore grid cell off the Estuary of Humber (EH, Fig. 9) shows a negative response, and a grid cell located at the frontal zone at the western edge of Dogger Bank (WDB, see Fig. 9) responds positively to spring-neap tidal forcing. The model results are presented for a couple of selected successive spring-neap tidal

515   cycles simulated for the year 2001 (Fig. 10).

Earth System
Dynamics
Discussions

The EH site, which is located further inshore compared to the WDB, is characterized by high turbidity. The increased nitrogen in the upper layers is in phase with elevated turbidity but in anti-phase with biomass and NPP. This phenomenon indicates that during spring tide, the process of phytoplankton biomass dilution (Fig. 10c) and shading due to the upward mixing of organic material (Fig. 10b) slows NPP in the upper mixed layer, resulting in a negative NPP response during

520 spring phases (Fig. 10d). The elevated NPP reaches a maximum at the end of the neap phase (Fig. 10d), possibly because of the reduced vertical mixing. The decreasing turbidity in the neap phases, despite increases in phytoplankton biomass, reveals that suspended and resuspended organic material have a reduced impact on the surface light conditions during neap phases compared to the spring phases (Fig. 10b). In neap tidal phase, given better light conditions, phytoplankton cells remain in the lighted surface layer for longer time; hence, the available nutrients can be utilized for phytoplankton growth.

525 In contrast, the WDB site is typically characterized by seasonal stratification and summer nutrient (i.e., nitrate) depletion in the surface layer. However, as the WBD site is located in the frontal zone, relevant factors in this zone do not necessarily show the spring-neap fluctuation as clearly as those in the EH site. Spring tidal forcing results in the replenishment of nutrients in the euphotic zone and a pulse of increased NPP follows spring tide mixing (Fig. 10e, h). The downward mixing of biomass into lower layers has no substantial negative effect on NPP during spring tide (Fig. 10g). As a consequence of

530 nutrient replenishment that fuels NPP in spring tides, biomass increases in the upper layers during neap tides (Fig. 10g). Resuspension effects resulting in increased turbidity at lower layers are visible from neap to spring but do not significantly change turbidity in the surface layers (Fig. 10f). Surface turbidity changes are consequences of increased NPP (Fig. 10f). Comparing our results with observations made by Richardson et al. (2000), which was taken at the northern edge of the Dogger Bank, our simulated response of NPP to tidal forcing at the northern edge of the Dogger Bank is 7.5 $gC\ m^{-2}y^{-1}$,

535 with a maximum of 20 $gC\ m^{-2}y^{-1}$ the southwestern boundary of Dogger Bank for the whole stratified season (Fig. 8). These values are at the lower edge of Richardson's estimate of 24-48 $gC\ m^{-2}$ from a rough upscaling of the observed nutrient injection to the pycnocline for the whole stratified season. Furthermore, in the Dogger Bank area, the surface layer NPP response (with a range of 10-30 $gC\ m^{-2}y^{-1}$ over the whole stratified season) (Fig. 8b) is more significant than the NPP response of the subsurface layer (no more than 7 $gC\ m^{-2}y^{-1}$ in the whole stratified season) (Fig. 8a), which contrasts with

540 Richardson's observation that nutrient injection mainly fuels the NPP in the subsurface layer. The subsurface NPP attributed to nitrate fluxes driven by spring-neap tides by Richardson et al. were 4-6 $gC\ m^{-2}$ for one spring-neap cycle, which is higher than our estimation of 0.26 $gC\ m^{-2}$ for one spring-neap cycle averaged across the whole stratified season. Based on our study, the limited influence of the spring-neap cycle indicates that the semidiurnal tide plays a major role in pumping up nutrients and sustaining the NPP, not only at the subsurface layer but also at the surface layer. The NPP in the present study

545 is likely lower than that in the study of Richardson's (Richardson et al., 2000) because seasonal variations in stratification change the thermocline depth and the position of the tidal mixing front. Moreover, upscaling must account for seasonality in bloom dynamics and light conditions. Conditions measured over a few days between July and August (Richardson et al., 2000)are not representative of those measured over the whole stratified season and therefore may not be appropriate for upscaling. Stratification during this short time period may be more stable than average climatological conditions, and

550 consequently, spring-neap tidal forcing may only impact subsurface NPP. All these aspects together limit the potential of linear upscaling. Based on our study, tidal pumping sustaining subsurface NPP mainly occurs in July and August, with an average value of approximately 3 $gC\ m^{-2}month^{-1}$ (not shown) in frontal areas around Dogger Bank, which is closer to the estimate of Richardsons et al. (2000). In other weakly stratified months, the value is no more than 1 $gC\ m^{-2}$ per month or even negative. In our simulation, the increased NPP caused by tidal forcing is closer to Richardson's observation for the

555 frontal zones in south and west of Dogger Bank. Here, we simulated a change of 6-8 $gC\ m^{-2}$ in the surface and 1-1.5 $gC\ m^{-2}$ in the subsurface for one spring neap cycle under strong stratified conditions. However, the additional contribution from the spring-neap cycle compared to M_2 tidal forcing is also not more than 1 $gC\ m^{-2}$ and thus rather limited.

Sharples (2008) investigated a similar question for the Celtic Sea with model simulations. He found that the NPP varied up to 70% with the spring-neap tidal cycle. We could not confirm such high tidal impacts on NPP for the North Sea; our

560 estimates of the response of NPP to the spring-neap tidal cycle are only up to approximately 10% of the tidal impact (M_2+S_2) on NPP (Fig. 2 & 9). One explanation for this discrepancy is the higher spring-neap tidal current amplitude in the Celtic Sea than that in the North Sea, which may result in a stronger response of NPP to the spring-neap cycle. However, it is also possible that the simpler model parameterizations used by Sharples, such as a constant grazing rate and neglected impacts on resuspension and shading by DOM and detritus, resulted in higher NPP sensitivity to tidal forcing in their simulation.

565 As discussed in section 3.2, tidal forcing not only impacts the magnitude of NPP but also spring bloom phenology. It is reasonable to assume that spring-neap tidal forcing also modulates the development of the spring bloom. To understand the impact of the spring-neap phase on the biomass build-up during the spring bloom, which typically occurs over one or several spring-neap cycles, we related the time periods with the maximum difference in NPP between the *tidal scenario* and the *M_2 scenario* to the spring-neap cycle phase (Fig. 11) at the SN site (see Fig. 9). The SN site is located in the tidally energetic

570 northwestern North Sea, where the development of the spring bloom often benefits from thermal stratification (Rodhe, 1998) but is sensitive to episodic 'noise' added by wind forcing (Waniek, 2003). During the development of the spring bloom, in the difference between NPP time series (*tidal scenario–M_2 scenario*), an increase in NPP often occurs in neap phases, whereas NPP is often decreased in spring phases. This indicates that the development of the spring bloom benefits from the neap phase but is interrupted or dampened during the spring tide (Fig. 11). A similar phenomenon has been explored and

575 confirmed by Sharples et al., (2006) at a site south of the SN site. As suggested by Sharples et al., (2006), the onset time of the spring bloom is shifted by the spring-neap tidal cycle because the onset or intensity of stratification is strengthened during neap tides when the vertical mixing is dampened.

4. Summary and Conclusions

A model-based sensitivity experiment with varied tidal forcing was performed to evaluate tidal impacts on NPP, considering

580 the major bottom-up controlling processes, including the tidal mixing of nutrients, organic matter and plankton biomass and tidal resuspension of suspended matter. The responses to tides in the North Sea differ regionally and depend on the local

hydrodynamic characteristics. In permanently mixed areas in the southern part of the North Sea, light availability is the major limiting factor. The enhanced tidal resuspension and mixing of suspended matter into the surface layers deteriorate light conditions in the upper layers for phytoplankton growth and thus hinder primary production. In contrast, in frontal areas

585   and seasonally stratified areas in the SNS where stratification is susceptible to tidal mixing, nutrient replenishment due to tidal forcing sustains NPP in summer and thus contributes a significant increase in NPP in both the surface layer and within the pycnocline. In the NNS, which is characterized by relatively weak tidal forcing and deep bathymetry, the bottom and upper mixed layers are well separated, and the influence of tidal forcing on NPP is limited.

However, the quantitative estimates provided here are model- and parameterization-specific. Dominant biochemical

590   processes are generally well represented in simplified NPZD-type models, and the ECOSMO model used here is applicable for resolving ecosystem dynamics at seasonal to decadal time scales when forced by realistic boundary conditions (Daewel and Schrum, 2017). However, parameterization and unconsidered processes, such as the role of macrobenthos in the system, internal waves at the shelf break, and coastal light attenuation due to inorganic suspended matter, and simplified physiological processes could potentially modulate or change the model's sensitivity to tidal forcing. Studies identifying the

595   contribution of these processes to tidal impacts on primary production are needed; thus far, we can only speculate on potential impacts.

Macrobenthic grazing likely changes the biochemical cycling and turbidity in the water column, subsequently changing the sensitivity of NPP to tidal forcing. In shallower waters, high near-bottom concentrations of suspended organic matter are susceptible to mixing into the euphotic zone, and increasing light attenuation leads to decreasing production (see Fig. 7c, cf.

600   section 3.1). Macrobenthic biomass, specifically from filter feeders, might significantly reduce resuspension and near-bottom suspended matter concentrations, thereby increasing the proportion of organic matter that remains in the food web (Prins et al., 1996). From observations, we know that macrobenthos show a distinct spatial pattern following principle production patterns in the North Sea with higher biomass in the shallow SNS (Heip et al., 1992). Therefore, we can expect an increase in NPP sensitivity to tidal forcing due to macrobenthos activity.

605   Furthermore, we hypothesize that the positive response of NPP to tidal forcing in the NNS was underestimated by our simulation due to the implementation of identical boundary conditions for all scenarios. We neglected the influence of tidal-generated internal waves on nutrient conditions. Tidal-generated internal waves are initiated at the shelf edge and enhance turbulent mixing at the shelf break and on the shelf (Heathershaw et al., 1987; Loder et al., 1992; New and Da Silva, 2002; Sharples et al., 2001). As internal tides break at the shelf edge, energy dissipates mainly at the shelf break and other

610   bathymetric features, which causes vertical mixing that drives vertical nutrient fluxes and sustains phytoplankton growth (Holligan et al., 1985; Pingree et al., 1981; Sharples et al., 2007). Therefore, internal tidal waves will likely lead to mixing and increase nutrient pulses onto the shelf, consequently supporting NPP. In our setup, the average impact of tidal-generated internal waves on nutrient concentrations was considered with the climatological boundary conditions (Conkright et al., 2002), and differences among the simulated scenarios were not considered.

615   Another source of uncertainty in our model stems from the neglect of inorganic material, which influences underwater light conditions, especially in shallow areas. Seasonal differences in yellow substance concentrations coincide with fresh water input (Schaub and Gieskes, 1991; Warnock et al., 1999). There are two main sources of SPM plumes in the North Sea. One source lies at the southern British coast and originates from local discharges (Humber-Wash & Thames rivers), coastal erosion and influx from the English Channel (Eisma, 2009). The other major source of SPM originates from the large rivers

620   and diffusive sources entering the North Sea from the European continental coast, particularly off the Belgian coast and the Wadden Sea (van Alphen, 1990; Postma, 1981). Waves and currents are the controlling factors of the dispersion, resuspension and deposition processes of SPM (Holt and James, 1999). In winter, the two SPM plumes expand further offshore due to intensified mixing and both SPM plume deposits in both the Skagerrak and Norwegian Channels. However, in stratified seasons, the concentration of SPM in the upper water layer decreases due to stratification, except for in shallow

625   areas with permanent mixing (Van Raaphorst et al., 1998). Thus, we can infer that the light conditions in shallow areas, especially in near-shore and permanently mixed regions, deteriorate due to tidal forcing and subsequently further decrease NPP in the *tidal scenario*. However, in farther offshore and seasonally stratified areas, this effect has little relevance for NPP.

    The major tidal impacts on NPP are via vertical mixing. Given the small horizontal gradient of both nutrients and biomass

630   and weak tidal residuals of no more than a few centimetres per second (Prandle, 1984), the impacts of horizontal advection are negligible. To investigate the influence of advection on the concentration of nutrients and phytoplankton biomass in our study, we estimated the net horizontal transport between grid cells. In most parts of the study domain, we found that the contribution of tidal advection does not exceed 5% (not shown here). Exceptions occur in the Skagerrak Channel, where relatively high residual currents drive water exchange between the North Sea and Baltic Sea (Brettschneider, 1967), and in

635   the EC close to the model boundary, where relatively high current speeds caused by atmospheric forcing and topography emerge irregularly, mainly in spring and winter. However, this result is not true for smaller horizontal and temporal resolutions.

    Given the importance of tidal forcing to NPP, especially in frontal areas, which are known to be biological hotspots (Belkin et al., 2009), tidal impacts on higher trophic levels than those studied here merit further consideration and investigation in the

640   future. Regarding the growth of macrobenthos, tidal stirring influences the sinking and resuspension of organic matter and thus influences food quality and bioturbation (Foshtomi et al., 2015; Zhang and Wirtz, 2017). Tidal forcing in frontal areas not only provides enough prey for fish larvae due to nutrient enrichment and higher NPP but also influences convergence zones, which are typical places for fish spawning and nursing (Bakun, 2006). Further investigations based on a combination of observations and multi-process coupled simulations could enable a better understanding of the impacts of tidal forcing on

645   ecosystem processes and their variability. Long-term tidal variations, such as the 18.61-year nodal cycle or the 8.85-year lunar perigee cycle, merit particular consideration.

Earth System
Dynamics
Discussions

Acknowledgements

655

660

665

670

675

680 **Reference**

Allen, J. I., Siddorn, J. R., Blackford, J. C. and Gilbert, F. J.: Turbulence as a control on the microbial loop in a temperate seasonally stratified marine systems model, J. Sea Res., 52(1), 1–20, doi:10.1016/j.seares.2003.09.004, 2004.

van Alphen, J. S. L. J.: A mud balance for Belgian-Dutch coastal waters between 1969 and 1986, Netherlands J. Sea Res., doi:10.1016/0077-7579(90)90005-2, 1990.

685 Tafeln der Astronomischen Argumente V0+v und der Korrektionen j,v, Deutsches Hydrographisches Insititut, Hamburg., 1967.

Arheimer, B., Dahné, J., Donnelly, C., Lindström, G. and Strömqvist, J.: Water and nutrient simulations using the HYPE model for Sweden vs. the Baltic Sea basin - Influence of input-data quality and scale, Hydrol. Res., 43(4), 315–329, doi:10.2166/nh.2012.010, 2012.

690 de Baar, H. J. W.: von Liebig's law of the minimum and plankton ecology (1899-1991), Prog. Oceanogr., doi:10.1016/0079-6611(94)90022-1, 1994.

Backhaus, J. O.: A three-dimensional model for the simulation of shelf sea dynamics, Dtsch. Hydrogr. Zeitschrift, 38(4), 165–187, 1985.

Backhaus, J. O. and Hainbucher, D.: A finite difference general circulation model for shelf seas and its application to low 695 frequency variability on the north european shelf, Elsevier Oceanogr. Ser., 45(C), 221–244, doi:10.1016/S0422-9894(08)70450-1, 1987.

Bagniewski, W., Fennel, K., Perry, M. J. and D'Asaro, E. A.: Optimizing models of the North Atlantic spring bloom using physical, chemical and bio-optical observations from a Lagrangian float, Biogeosciences, doi:10.5194/bg-8-1291-2011, 2011.

700 Bakun, A.: Fronts and eddies as key structures in the habitat of marine fish larvae: opportunity, adaptive response and competitive advantage, Sci. Mar., doi:10.3989/scimar.2006.70s2105, 2006.

Balch, W. M. K.: An apparent lunar tidal cycle of phytoplankton blooming and community succession in the Gulf of Maine, J. Exp. Mar. Bio. Ecol., 55(1), 65–77, doi:10.1016/0022-0981(81)90093-9, 1981.

Barthel, K., Daewel, U., Pushpadas, D., Schrum, C., Arthun, M. and Wehde, H.: Resolving frontal structures: On the payoff 705 using a less diffusive but computationally more expensive advection scheme, Ocean Dyn., 62(10–12), 1457–1470, doi:10.1007/s10236-012-0578-9, 2012.

Belkin, I. M., Cornillon, P. C. and Sherman, K.: Fronts in Large Marine Ecosystems, Prog. Oceanogr., 81(1–4), 223–236, doi:10.1016/j.pocean.2009.04.015, 2009.

Benoit-Bird, K. J., Cowles, T. J. and Wingard, C. E.: Edge gradients provide evidence of ecological interactions in 710 planktonic thin layers, Limnol. Oceanogr., 54(4), 1382–1392, doi:10.4319/lo.2009.54.4.1382, 2009.

Van Beusekom, J., Diel-Christiansen, A.: Synthesis of phyto- and zooplankton dynamics in the North Sea environment 148 pp, Godalming., 1994.

Earth System
Dynamics
Discussions

Blauw, A. N., Benincà, E., Laane, R. W. P. M., Greenwood, N. and Huisman, J.: Dancing with the Tides: Fluctuations of Coastal Phytoplankton Orchestrated by Different Oscillatory Modes of the Tidal Cycle, PLoS One, 7(11),

715   doi:10.1371/journal.pone.0049319, 2012.

Bowden, K. F. and Hamilton, P.: Some experiments with a numerical model of circulation and mixing in a tidal estuary, Estuar. Coast. Mar. Sci., doi:10.1016/0302-3524(75)90029-8, 1975.

Bowers, D. G., Boudjelas, S. and Harker, G. E. L.: The distribution of fine suspended sediments in the surface waters of the irish sea and its relation to tidal stirring, Int. J. Remote Sens., doi:10.1080/014311698214514, 1998.

720   Brettschneider, G.: Anwendung des hydrodynamisch-numerischen Verfahrens zur Ermittlung der M2-Mitschwingungsgezeit der Nordsee, Univ. Hamburg., 1967.

Cloern, J. E.: Tidal Stirring and Phytoplankton Bloom Dynamics in an Estuary, J. Mar. Res., 49(1), 203–221, doi:10.1357/002224091784968611, 1991.

Conkright, M. E., Locarnini, R. a, Garcia, H. E., O'Brien, T. D., Boyer, T. P., Stepens, C. and Antonov, J. I.: World Ocean

725   Atlas 2001: Objective analyses, data statistics, and figures CD-ROM documentation, Natl. Oceanogr. Data Cent. Intern. Rep. (NOAA   Atlas   NESDIS),   17(September),   17   [online]   Available   from: http://www.nodc.noaa.gov/OC5/WOA01/pr_woa01.html, 2002.

Cullen, J. J.: Subsurface chlorophyll maximum layers: enduring enigma or mystery solved?, Ann. Rev. Mar. Sci., 7, 207–39, doi:10.1146/annurev-marine-010213-135111, 2015.

730   Daewel, U. and Schrum, C.: Simulating long-term dynamics of the coupled North Sea and Baltic Sea ecosystem with ECOSMO II: Model description and validation, J. Mar. Syst., 119–120, 30–49, doi:10.1016/j.jmarsys.2013.03.008, 2013.

Daewel, U. and Schrum, C.: Low frequency variability in North Sea and Baltic Sea identified through simulations with the 3-d coupled physical-biogeochemical model ECOSMO, Earth Syst. Dyn. Discuss., (April), 1–23, doi:10.5194/esd-2017-36, 2017.

735   Daewel, U., Hjøllo, S. S., Huret, M., Ji, R., Maar, M., Niiranen, S., Travers-Trolet, M., Peck, M. A. and Van De Wolfshaar, K. E.: Predation control of zooplankton dynamics: A review of observations and models, ICES J. Mar. Sci., doi:10.1093/icesjms/fst125, 2014.

Daly, K. L. and Smith, W. O.: Physical-Biological Interactions Influencing Marine Plankton Production, Annu. Rev. Ecol. Syst., doi:10.1146/annurev.es.24.110193.003011, 1993.

740   Davies, A. M. and Lawrence, L.: Modelling the Non-linear Interaction of Wind and Tide: Its Influence on Current Profiles, Int. J. Numer. Methods fluids, 18(March 1993), 163–188, 1994.

Davies, A. M., Sauvel, J. and Evans, J.: Computing near coastal tidal dynamics from observations and a numerical model, Cont. Shelf Res., 4(3), 341–366 [online] Available from: https://doi.org/10.1016/0278-4343(85)90047-0, 1985.

Dekshenieks, M. M., Donaghay, P. L., Sullivan, J. M., Rines, J. E. B., Osborn, T. R. and Twardowski, M. S.: Temporal and

745   spatial occurrence of thin phytoplankton layers in relation to physical processes, Mar. Ecol. Prog. Ser., 223, 61–71, doi:10.3354/meps223061, 2001.

Dippner, J. W.: A frontal-resolving model for the German Bight, Cont. Shelf Res., doi:10.1016/0278-4343(93)90035-V, 1993.

Ebenhöh, W., Kohlmeier, C., Baretta, J. W. and Flöser, G.: Shallowness may be a major factor generating nutrient gradients in the Wadden Sea, Ecol. Modell., doi:10.1016/j.ecolmodel.2003.07.011, 2004.

Eisma, D.: Supply and Deposition of Suspended Matter in the North Sea, in Holocene Marine Sedimentation in the North Sea Basin, pp. 415–428., 2009.

Eliasen, S. K., Hátún, H., Larsen, K. M. H., Hansen, B. and Rasmussen, T. A. S.: Phenologically distinct phytoplankton regions on the Faroe Shelf - identified by satellite data, in-situ observations and model, J. Mar. Syst., 169, 99–110, doi:10.1016/j.jmarsys.2017.01.015, 2017.

Foshtomi, M. Y., Braeckman, U., Derycke, S., Sapp, M., Van Gansbeke, D., Sabbe, K., Willems, A., Vincx, M. and Vanaverbeke, J.: The link between microbial diversity and nitrogen cycling in marine sediments is modulated by macrofaunal bioturbation, PLoS One, 10(6), 1–20, doi:10.1371/journal.pone.0130116, 2015.

Franks, P. J. S. and Chen, C.: Plankton production in tidal fronts: A model of Georges Bank in summer, J. Mar. Res., 54(4), 631–651, doi:10.1357/0022240963213718, 1996.

George, J. A., Lonsdale, D. J., Merlo, L. R. and Gobler, C. J.: The interactive roles of temperature, nutrients, and zooplankton grazing in controlling the winter-spring phytoplankton bloom in a temperate, coastal ecosystem, Long Island Sound, Limnol. Oceanogr., doi:10.1002/lno.10020, 2015.

Geyer, W. R. and MacCready, P.: The Estuarine Circulation, Annu. Rev. Fluid Mech., 46(1), 175–197, doi:10.1146/annurev-fluid-010313-141302, 2014.

Heathershaw, a. D., New, a. L. and Edwards, P. D.: Internal tides and sediment transport at the shelf break in the Celtic Sea, Cont. Shelf Res., 7(5), 485–517, doi:10.1016/0278-4343(87)90092-6, 1987.

Heip, C., Basford, D., Craeymeersch, J. A., Dewarumez, J., Dörjes, J., Wilde, P. De, Duineveld, G., Eleftheriou, A., Herman, P. M. J., Niermann, U., Kingston, P., Künitzer, A., Rachor, E., Rumohr, H., Soetaert, K. and Soltwedel, T.: Trends in biomass , density and diversity of North Se a macrofauna, , 13–22, 1992.

Henriksen, H. J., Troldborg, L., Nyegaard, P., Sonnenborg, T. O., Refsgaard, J. C. and Madsen, B.: Methodology for construction, calibration and validation of a national hydrological model for Denmark, J. Hydrol., doi:10.1016/S0022-1694(03)00186-0, 2003.

Hofmeister, R., Flöser, G. and Schartau, M.: Estuary-type circulation as a factor sustaining horizontal nutrient gradients in freshwater-influenced coastal systems, Geo-Marine Lett., 37(2), 179–192, doi:10.1007/s00367-016-0469-z, 2017.

Holligan, P. M., Pingree, R. D. and Mardell, G. T.: Oceanic solitons, nutrient pulses and phytoplankton growth, Nature, 314(6009), 348–350, doi:10.1038/314348a0, 1985.

Holt, J., Butenschön, M., Wakelin, S. L., Artioli, Y. and Allen, J. I.: Oceanic controls on the primary production of the northwest European continental shelf: Model experiments under recent past conditions and a potential future scenario, Biogeosciences, 9(1), 97–117, doi:10.5194/bg-9-97-2012, 2012.

Holt, J. T. and James, I. D.: A simulation of the southern North Sea in comparison with measurements from the North Sea Project Part 2 suspended particulate matter, Cont. Shelf Res., 19(12), 1617–1642, doi:10.1016/S0278-4343(99)00032-1, 1999.

Hu, S., Townsend, D. W., Chen, C., Cowles, G., Beardsley, R. C., Ji, R. and Houghton, R. W.: Tidal pumping and nutrient
785   fluxes on Georges Bank: A process-oriented modeling study, J. Mar. Syst., 74(1–2), 528–544, doi:10.1016/j.jmarsys.2008.04.007, 2008.

Jacob, B. and Stanev, E. V.: Interactions between wind and tidally induced currents in coastal and shelf basins, Ocean Dyn., 67(10), 1263–1281, doi:10.1007/s10236-017-1093-9, 2017.

Jacobs, W.: Modelling the Rhine River Plume, TU Delft., 2004.

790   Jago, C. F., Jones, S. E., Latter, R. J., McCandliss, R. R., Hearn, M. R. and Howarth, M. J.: Resuspension of benthic fluff by tidal currents in deep stratified waters, northern North sea, in Journal of Sea Research., 2002.

Janssen, F., Schrum, C. and Backhaus, J. O.: A climatological data set of temperature and salinity for the Baltic Sea and the North Sea, Dtsch. Hydrogr. Zeitschrift, 51(9), 5, doi:10.1007/BF02933676, 1999.

Janssen, F., Schrum, C., Hübner, U. and Backhaus, J. O.: Uncertainty analysis of a decadal simulation with a regional ocean
795   model for the North Sea and Baltic Sea, Clim. Res., 18(1–2), 55–62, doi:10.3354/cr018055, 2001.

Joint, I. and Pomroy, A.: Phytoplankton Biomass and Production in the Southern North-Sea, Mar. Ecol. Ser., 1993.

Joint, T. and Pomroy, A.: hytoplankton Biomass and Production in the North Sea. Results from the NERC North Sea Project August 1988-October 1989, Plymouth., 1992.

Kalnay, E., Kanamitsu, M., Kistler, R., Collins, W., Deaven, D., Gandin, L., Iredell, M., Saha, S., White, G., Woollen, J.,
800   Zhu, Y., Chelliah, M., Ebisuzaki, W., Higgins, W., Janowiak, J., Mo, K. C., Ropelewski, C., Wang, J., Leetmaa, A., Reynolds, R., Jenne, R. and Joseph, D.: The NCEP/NCAR 40-year reanalysis project, Bull. Am. Meteorol. Soc., 77(3), 437–471, doi:10.1175/1520-0477(1996)077<0437:TNYRP>2.0.CO;2, 1996.

van Leeuwen, S. M., van der Molen, J., Ruardij, P., Fernand, L. and Jickells, T.: Modelling the contribution of deep chlorophyll maxima to annual primary production in the North Sea, Biogeochemistry, 113(1–3), 137–152,
805   doi:10.1007/s10533-012-9704-5, 2013.

Van Leeuwen, S., Tett, P., Mills, D. and Van Der Molen, J.: Stratified and nonstratified areas in the North Sea: Long-term variability and biological and policy implications, J. Geophys. Res. C Ocean., 120(7), 4670–4686, doi:10.1002/2014JC010485, 2015.

Lindström, G., Pers, C., Rosberg, J., Strömqvist, J. and Arheimer, B.: Development and testing of the HYPE (Hydrological
810   Predictions for the Environment) water quality model for different spatial scales, Hydrol. Res., 43(3–4), 295–319, doi:10.2166/nh.2010.007, 2010.

Loder, J. W. and Greenberg, D. A.: Predicted positions of tidal fronts in the Gulf of Maine region, Cont. Shelf Res., doi:10.1016/0278-4343(86)90080-4, 1986.

Loder, J. W., Brickman, D. and Horne, E. P. W.: Detailed structure of currents and hydrography on the northern side of

815   Georges Bank, J. Geophys. Res., doi:10.1029/92JC01342, 1992.

Longhurst, A. R.: Ecological Geography of the Sea, Academic Press., 2006.

Mahadevan, A., Tandon, A. and Ferrari, R.: Rapid changes in mixed layer stratification driven by submesoscale instabilities and winds, J. Geophys. Res. Ocean., 115(3), 1–12, doi:10.1029/2008JC005203, 2010.

Martin, J. H.: PHYTOPLANKTON-ZOOPLANKTON RELATIONSHIPS IN NARRAGANSETT BAY, Limnol.
820   Oceanogr., 10(2), 185–191, 1965.

Matthias, V., Aulinger, A. and Quante, M.: Adapting CMAQ to investigate air pollution in North Sea coastal regions, Environ. Model. Softw., 23(3), 356–368, doi:10.1016/j.envsoft.2007.04.010, 2008.

McCandliss, R. R., Jones, S. E., Hearn, M., Latter, R. and Jago, C. F.: Dynamics of suspended particles in coastal waters (southern North Sea) during a spring bloom, J. Sea Res., 47(3–4), 285–302, doi:10.1016/S1385-1101(02)00123-5, 2002.

825   McQuatters-Gollop, A., Raitsos, D. E., Edwards, M. and Attrill, M. J.: Spatial patterns of diatom and dinoflagellate seasonal cycles in the NE Atlantic Ocean, Mar. Ecol. Prog. Ser., doi:10.3354/meps339301, 2007.

Monod, J.: Recherches sur la croissance des cultures bactériennes, Paris, Hermann & cie, 1942., 1942.

New, A. L. and Da Silva, J. C. B.: Remote-sensing evidence for the local generation of internal soliton packets in the central Bay of Biscay, Deep. Res. Part I Oceanogr. Res. Pap., doi:10.1016/S0967-0637(01)00082-6, 2002.

830   Otto, L., Zimmerman, J. T. F., Furnes, G. K., Mork, M., Saetre, R. and Becker, G.: Review of the physical oceanography of the North Sea, Netherlands J. Sea Res., 26(2–4), 161–238, doi:10.1016/0077-7579(90)90091-T, 1990.

Pätsch, J., Lenhart, H. J.: Daily Loads of Nutrients, Total Alkalinity, Dissolved Inorganic Carbon and Dissolved Organic Carbon of the European continental rivers for the years 1977–2002., 2004.

Pedersen, F. B.: The Oceanographic and Biological Tidal Cycle Succession in Shallow Sea Fronts in the North Sea and the
835   English Channel, Estuar. Coast. Shelf Sci., 38(3), 249–269, doi:10.1006/ecss.1994.1017, 1994.

Pietrzak, J. D., de Boer, G. J. and Eleveld, M. A.: Mechanisms controlling the intra-annual mesoscale variability of SST and SPM in the southern North Sea, Cont. Shelf Res., 31(6), 594–610, doi:10.1016/j.csr.2010.12.014, 2011.

Pingree, R. D. and Griffiths, D. K.: Tidal fronts on the shelf seas around the British Isles, J. Geophys. Res., 83(C9), 4615, doi:10.1029/JC083iC09p04615, 1978.

840   Pingree, R. D., Mardell, G. T. and Cartwright, D. E.: Slope Turbulence, Internal Waves and Phytoplankton Growth at the Celtic Sea Shelf-Break [and Discussion], Philos. Trans. R. Soc. A Math. Phys. Eng. Sci., 302(1472), 663–682, doi:10.1098/rsta.1981.0191, 1981.

Pohlmann, T.: Predicting the thermocline in a circulation model of the North Sea - Part I: Model description, calibration and verification, Cont. Shelf Res., 16(2), 131–146, doi:DOI: 10.1016/0278-4343(95)90885-S, 1996.

845   Porter, E. T., Mason, R. P. and Sanford, L. P.: Effect of tidal resuspension on benthic-pelagic coupling in an experimental ecosystem study, Mar. Ecol. Prog. Ser., doi:10.3354/meps08709, 2010.

Postma, H.: Exchange of materials between the North Sea and the Wadden Sea, Mar. Geol., doi:10.1016/0025-3227(81)90050-5, 1981.

850 Prins, T. C., Smaal, A. C., Pouwer, A. J. and Dankers, N.: Filtration and resuspension of particulate matter and phytoplankton onan intertidal mussel bed in the Oosterschelde estuary (SW Netherlands), Mar. Ecol. Prog. Ser., doi:10.3354/meps142121, 1996.

Van Raaphorst, W., Philippart, C. J. M., Smit, J. P. C., Dijkstra, F. J. and Malschaert, J. F. P.: Distribution of suspended particulate matter in the North Sea as inferred from NOAA/AVHRR reflectance images and in situ observations, J. Sea Res., 39(3–4), 197–215, doi:10.1016/S1385-1101(98)00006-9, 1998.

855 Richardson, K., Visser, A. and Pedersen, F.: Subsurface phytoplankton blooms fuel pelagic production in the North Sea, J. Plankton Res., 22(9), 1663–1671, doi:10.1093/plankt/22.9.1663, 2000.

Rodhe, J.: The Baltic and Northern Seas: a process-orientated review of the physical oceanography., in The sea, edited by A. R. Robinson and K. H. Brink, pp. 699–732, Wildy, New York., 1998.

Rodhe, J., Tett, P. and Wulf, F.: Chapter 26 . The Baltic and North Seas: a regional review of some important physical - 860 checmial-biological interaction processes, Sea, 14, 1029–1072, 2004.

Ruddick, K. G., Deleersnijder, E., Luyten, P. J. and Ozer, J.: Haline stratification in the Rhine-Meuse freshwater plume: a three-dimensional model sensitivity analysis, Cont. Shelf Res., doi:10.1016/0278-4343(95)00034-X, 1995.

Sabine, C. L., Feely, R. A., Gruber, N., Key, R. M., Lee, K., Bullister, J. L., Wanninkhof, R., Wong, C. S., Wallace, D. W. R., Tilbrook, B., Millero, F. J., Peng, T. H., Kozyr, A., Ono, T. and Rios, A. F.: The oceanic sink for anthropogenic CO2, 865 Science (80-.)., 305(5682), 367–371, doi:10.1126/science.1097403, 2004.

Schaub, B.E.M., Gieskes, W. W. C.: Eutrophication of the North Sea: the relation between Rhine river discharge and chlorophyll-a concentration in Dutch coastal waters, Fredensborg., 1991.

Schrum, C.: Thermohaline stratification and instabilities at tidal mixing fronts: Results of an eddy resolving model for the German Bight, Cont. Shelf Res., 17(6), 689–716, doi:10.1016/S0278-4343(96)00051-9, 1997.

870 Schrum, C. and Backhaus, J. O.: Sensivity of atmosphere-ocean heat exchange and heat content in the North Sea and the Baltic Sea, Tellus, 51A, 526–549, doi:10.1034/j.1600-0870.1992.00006.x, 1999.

Schrum, C., Siegismund, F. and John, M. S.: Decadal variations in the stratification and circulation patterns of the North Sea. Are the 1990s unusual?, ICES Mar. Sci. Symp., 2003.

Schrum, C., St. John, M. and Alekseeva, I.: ECOSMO, a coupled ecosystem model of the North Sea and Baltic Sea: Part II. 875 Spatial-seasonal characteristics in the North Sea as revealed by EOF analysis, J. Mar. Syst., 61(1–2), 100–113, doi:10.1016/j.jmarsys.2006.01.004, 2006.

Scott, B. E., Sharples, J., Ross, O. N., Wang, J., Pierce, G. J. and Camphuysen, C. J.: Sub-surface hotspots in shallow seas: Fine-scale limited locations of top predator foraging habitat indicated By tidal mixing and sub-surface chlorophyll, Mar. Ecol. Prog. Ser., 408, 207–226, doi:10.3354/meps08552, 2010.

880 Sea, I. C. for the E. of the: Flushing times of the North Sea, Copenhagen., 1983.

Sharples, J.: Potential impacts of the spring-neap tidal cycle on shelf sea primary production, J. Plankton Res., 30(2), 183–197, doi:10.1093/plankt/fbm088, 2008.

Earth System
Dynamics
Discussions

Sharples, J. and Simpson, J. H.: Periodic Frontogenesis in a Region of Freshwater Influence, Estuaries, 16(1), 74, doi:10.2307/1352765, 1993.

885 Sharples, J., Moore, M. C., Rippeth, T. P., Holligan, P. M., Hydes, D. J., Fisher, N. R. and Simpson, J. H.: Phytoplankton distribution and survival in the thermocline, Limnol. Oceanogr., doi:10.4319/lo.2001.46.3.0486, 2001.

Sharples, J., Ross, O. N., Scott, B. E., Greenstreet, S. P. R. and Fraser, H.: Inter-annual variability in the timing of stratification and the spring bloom in the North-western North Sea, Cont. Shelf Res., 26(6), 733–751, doi:10.1016/j.csr.2006.01.011, 2006.

890 Sharples, J., Tweddle, J. F., Green, J. A. M., Palmer, M. R., Kim, Y., Hickman, A. E., Holligan, P. M., Moore, C. M., Rippeth, T. P., Simpson, J. H. and Krivtsov, V.: Spring – neap modulation of internal tide mixing and vertical nitrate fluxes at a shelf edge in summer, , 52(5), 1735–1747, 2007.

Siegismund, F.: Long-term changes in the flushing times of the ICES-boxes, Senckenbergiana maritima, 31(2), 151–167, doi:10.1007/BF03043025, 2001.

895 Simpson, J., J. H. S.: Introduction to the Physical and Biological Oceanography of Shelf Seas, Cambridge University Press., 2012.

Simpson, J. H. and Bowers, D.: Models of stratification and frontal movement in shelf seas, Deep Sea Res. Part A, Oceanogr. Res. Pap., doi:10.1016/0198-0149(81)90132-1, 1981.

Simpson, J. H. and Hunter, J. R.: Fronts in the Irish Sea, Nature, 250(5465), 404–406, doi:10.1038/250404a0, 1974.

900 Simpson, J. H. and Souza, A. J.: Semidiurnal switching of stratification in the region of freshwater influence of the Rhine, J. Geophys. Res., doi:10.1029/95JC00067, 1995.

Smith, W. O. and Jones, R. M.: Vertical mixing, critical depths, and phytoplankton growth in the Ross Sea, ICES J. Mar. Sci., doi:10.1093/icesjms/fsu234, 2015.

Stedmon, C. A., Markager, S. and Kaas, H.: Optical Properties and Signatures of Chromophoric Dissolved Organic Matter 905 (CDOM) in Danish Coastal Waters, Estuar. Coast. Shelf Sci., doi:10.1006/ecss.2000.0645, 2000.

Stoica, P., Moses, R. L. and Hall, P.: Introduction to Spectral Analysis, Technometrics, doi:10.1198/tech.2005.s841, 2005.

Tett, P. and Walne, A.: Observations and simulations of hydrography, nutrients and plankton in the southern north sea, Ophelia, 42(1), 371–416, doi:10.1080/00785326.1995.10431514, 1995.

Thomson, R. E. and Emery, W. J.: Chapter 5 - Time Series Analysis Methods, edited by R. E. Thomson and W. J. B. T.-D. 910 A. M. in P. O. (Third E. Emery, pp. 425–591, Elsevier, Boston., 2014.

Tian, T., Merico, A., Su, J., Staneva, J., Wiltshire, K. and Wirtz, K.: Importance of resuspended sediment dynamics for the phytoplankton spring bloom in a coastal marine ecosystem, J. Sea Res., 62(4), 214–228, doi:10.1016/j.seares.2009.04.001, 2009.

Urtizberea, A., Dupont, N., Rosland, R. and Aksnes, D. L.: Sensitivity of euphotic zone properties to CDOM variations in 915 marine ecosystem models, Ecol. Modell., doi:10.1016/j.ecolmodel.2013.02.010, 2013.

Waniek, J. J.: The role of physical forcing in initiation of spring blooms in the northeast Atlantic, J. Mar. Syst.,

Earth System Dynamics
Discussions
Open Access
EGU

doi:10.1016/S0924-7963(02)00248-8, 2003.

Warnock, R. E., Gieskes, W. W. C. and Van Laar, S.: Regional and seasonal differences in light absorption by yellow substance in the Southern Bight of the North Sea, J. Sea Res., 42(3), 169–178, doi:10.1016/S1385-1101(99)00025-8, 1999.

920   Welch, P. D.: The use of fast Fourier transform for the estimation of power spectra: A method based on time averaging over short, modified periodograms, IEEE Trans. audio Electroacoust., doi:10.1109/TAU.1967.1161901, 1967.

Windolf, J., Thodsen, H., Troldborg, L., Larsen, S. E., Bøgestrand, J., Ovesen, N. B. and Kronvang, B.: A distributed modelling system for simulation of monthly runoff and nitrogen sources, loads and sinks for ungauged catchments in Denmark, J. Environ. Monit., doi:10.1039/c1em10139k, 2011.

925   Windolf, J., Blicher-Mathiesen, G., Carstensen, J. and Kronvang, B.: Changes in nitrogen loads to estuaries following implementation of governmental action plans in Denmark: A paired catchment and estuary approach for analysing regional responses, Environ. Sci. Policy, doi:10.1016/j.envsci.2012.08.009, 2012.

van der Woerd, H. J., Blauw, A., Peperzak, L., Pasterkamp, R. and Peters, S.: Analysis of the spatial evolution of the 2003 algal bloom in the Voordelta (North Sea), J. Sea Res., doi:10.1016/j.seares.2010.09.007, 2011.

930   Yee, H. C., Warming, R. F. and Harten, A.: Implicit total variation diminishing (TVD) schemes for steady-state calculations, J. Comput. Phys., doi:10.1016/0021-9991(85)90183-4, 1985.

Zhang, W. and Wirtz, K.: Mutual Dependence Between Sedimentary Organic Carbon and Infaunal Macrobenthos Resolved by Mechanistic Modeling, J. Geophys. Res. Biogeosciences, 122(10), 2509–2526, doi:10.1002/2017JG003909, 2017.

935

940

945

Earth System
Dynamics
Discussions

Table

Table 1 Average annual NPP and relative difference between the *tidal* and *non-tidal scenarios* in each

subdomain and in the entire North Sea.

Subdomain	Non-tidal scen. NPP(gCm^2y^{-1})	Tidal scen. NPP(gCm^2y^{-1})	Rel. Diff (%)
EC	125.2	97.2	-29%
neg. SNS	114.5	101.6	-13%
pos. SNS	93.3	118.8	21%
BC	121.0	135.3	11%
deep NNS	93.8	82.6	-14%
NT	97.7	106.4	9%
non-sen. NNS	92.3	94.5	2%
Total	100.7	103.2	3%

Earth System
Dynamics
Discussions
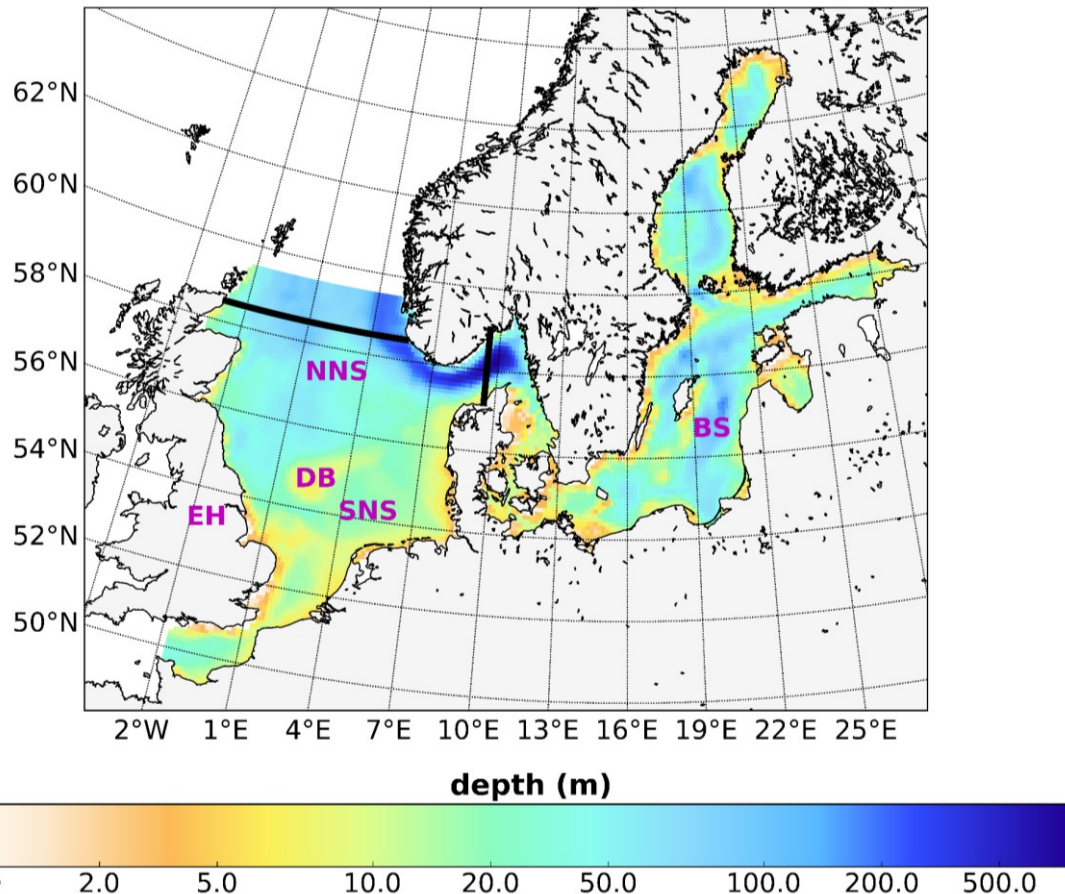
Figures

Figure 1. Bathymetry and simulation domain of ECOSMO. Black lines indicate the area of the North Sea used for analysis, from 5°W–9.5°E in the east-west direction and from 48°N-58.5°N in the south-north direction. SNS and NNS are short for the southern and northern North Sea, respectively. BS is short for the Baltic Sea. DB and EH are short for the Dogger Bank and the Estuary of Humber, respectively.
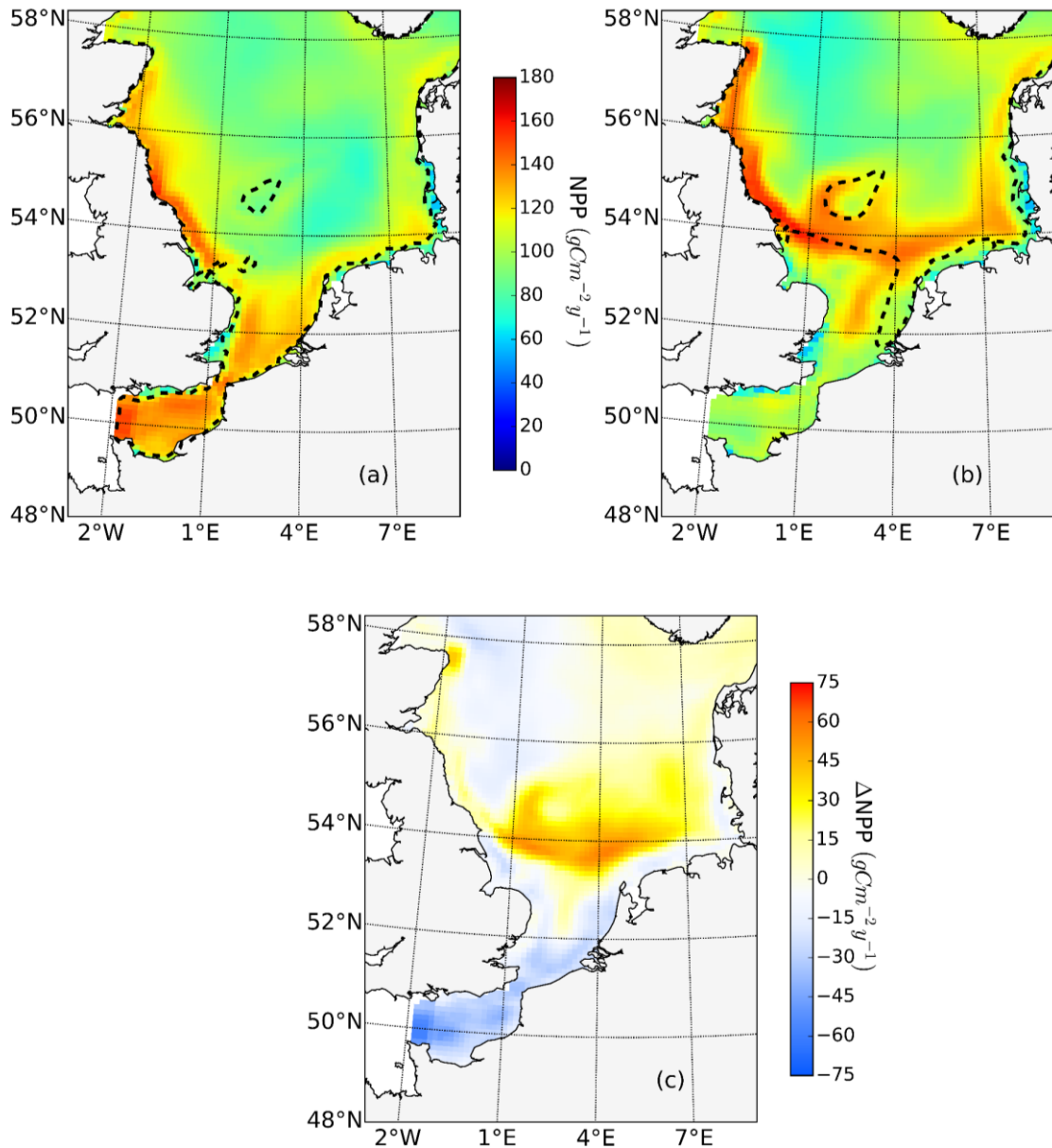
Figure 2. Mean annual net primary production for the *analysed period* (1990-2015) of the *non-tidal scenario* (a), *tidal scenario* (b) and the difference in the mean annual NPP of both scenarios (c). Dashed lines indicate the boundary between stratified (off-shore) and unstratified (near-shore, Dogger Bank) regions. The criterion for stratification is that squared buoyancy frequency N^2 remains higher than 0.013 for more than 60 days per year on average.
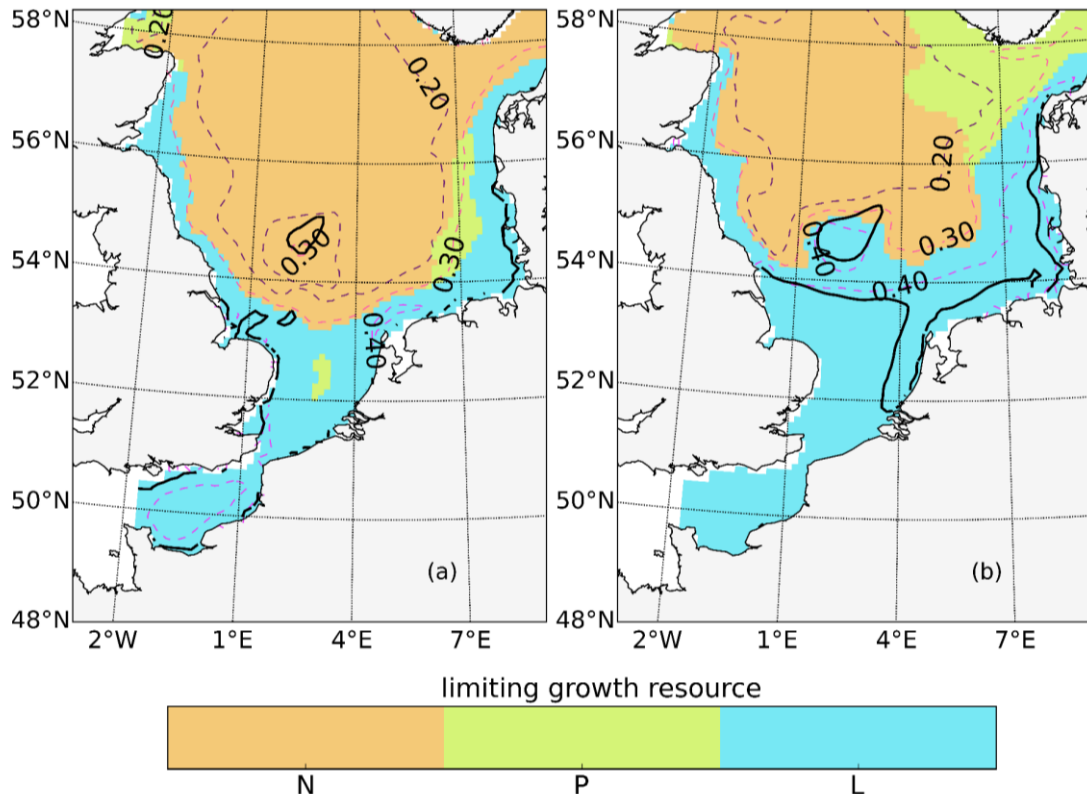
Figure 3. Mean values of the most limiting resources (N: nitrogen, P: phosphorus, L: light) in the surface layer for July (averaged for the *analysed period* 1990-2015) for the *non-tidal scenario* (a) and *tidal scenario* (b). The limiting value (derived from Liebig's law) is indicated by dashed contour lines. Stratified and unstratified areas are separated by black lines (definition see Fig. 2).

Earth System
Dynamics
Discussions
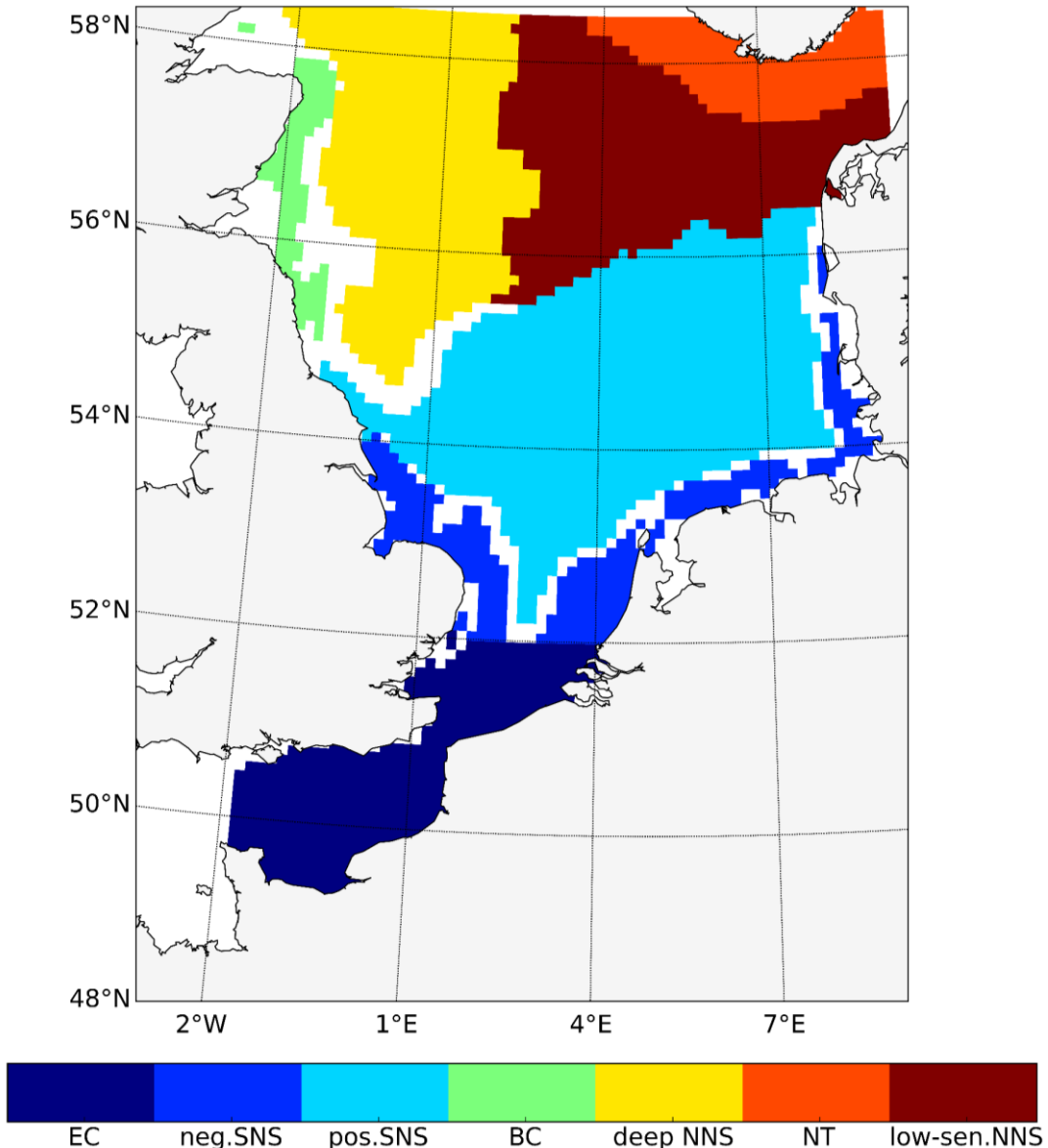
Figure 4. Process-oriented subdomain division of the North Sea based on tidally induced changes in net primary production and bathymetric characteristics (*EC*: English Channel, *neg. SNS*: negatively responding southern North Sea, *pos. SNS*: positively responding southern North Sea, *BC*- eastern British coast, *deep NNS:* deeper northern North Sea, *NT:* Norwegian Trench, *low-sen. NNS*: low-sensitivity northern North Sea. Areas with an absolute variation in NPP less than 5 $gCm^{-2}y^{-1}$ are excluded, except for the *low-sen. NNS* areas.
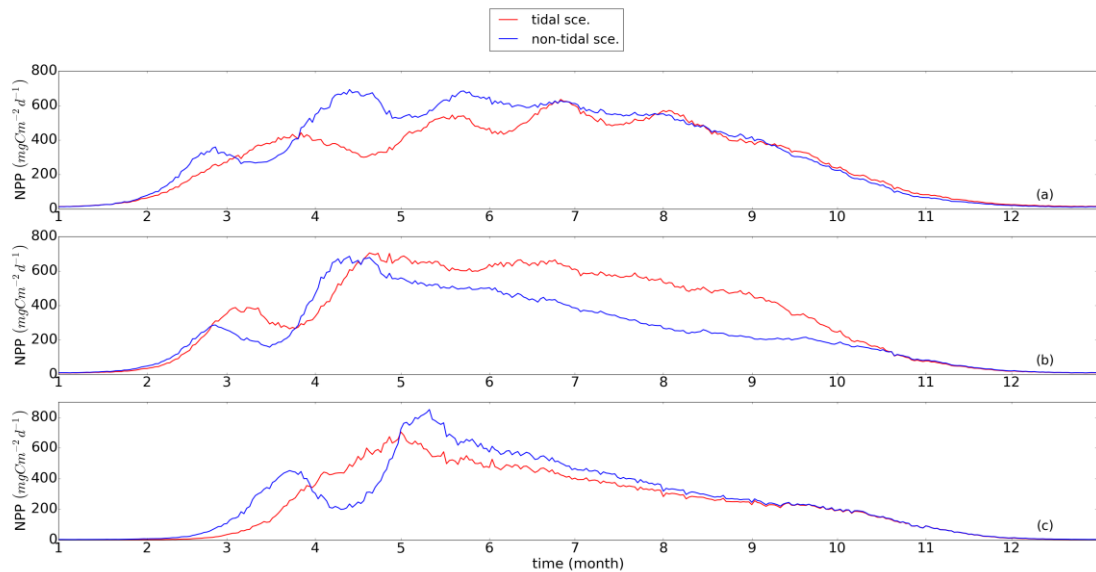
1005

Figure 5. Time series of averaged NPP (blue: non-tidal scenario, red: tidal scenario) in subdomains. a) neg.SNS: negatively responding southern North Sea, b) pos.SNS: positively responding southern North Sea and c) deep NNS: deeper northern North Sea. The NPP is averaged for the *analysed period* (1990-2015).

1010

1015

1020

35
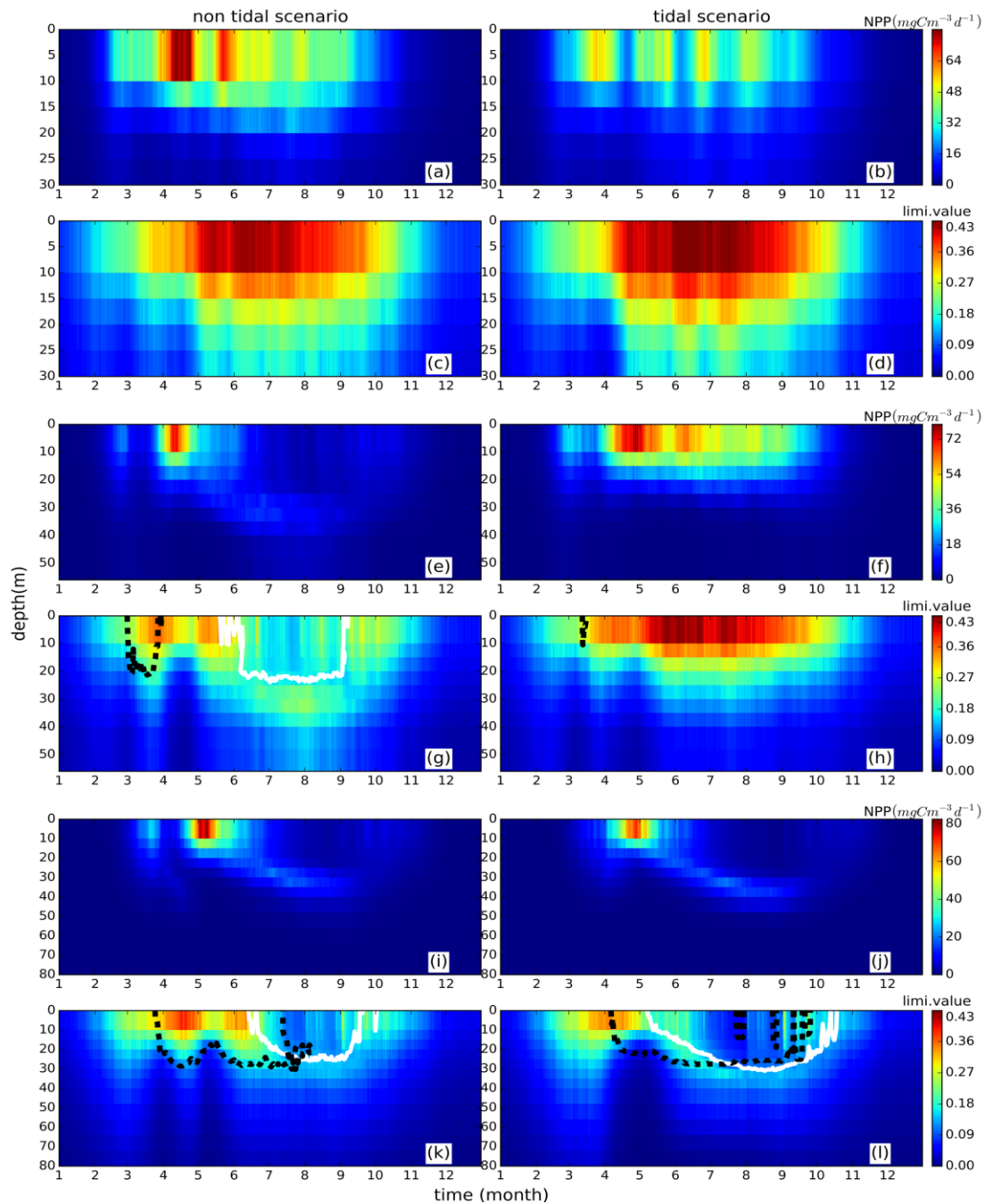
Figure 6. Time series of averaged (1990-2015) NPP vertical profiles (upper panels for each representative grid cell) and the limiting value (lower panel for each representative grid cell) for the *tidal* (right) and *non-tidal* (left) *scenarios*. NPP and limiting values are presented as the mean of each representative point for 3subdomains, i.e., *neg.SNS*, the negatively responding southern North Sea (a-d), *pos.SNS*, the positively responding southern North Sea (e-h) and *deep NNS*, the deeper northern North Sea (i-l). Additionally, the depth above which a specific nutrient (silicate: black solid line, nitrogen: white dashed line) is limiting to NPP is given.

Earth System
Dynamics
Discussions
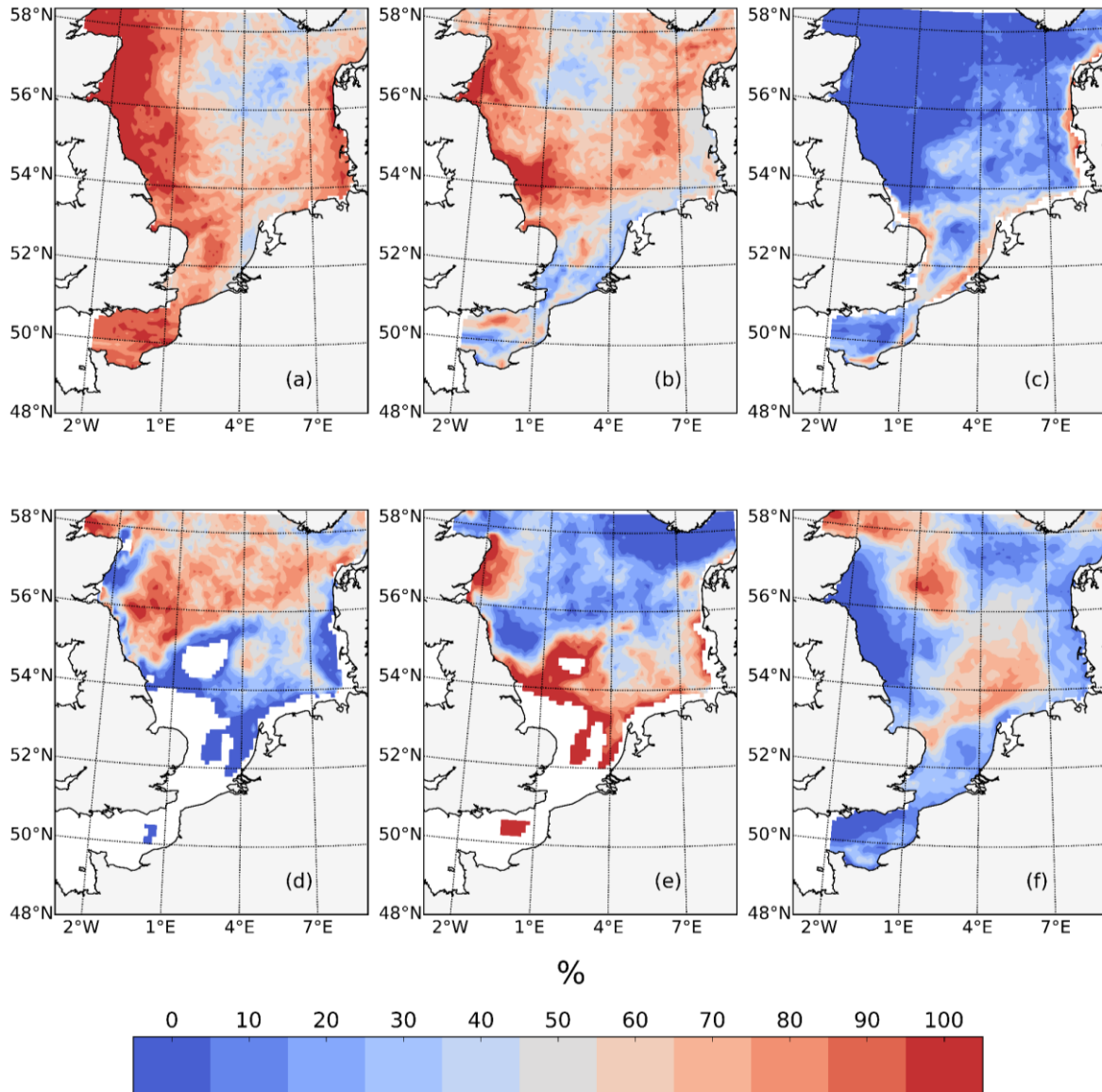
Figure 7. The percentage of years (1990-2015) in which specific processes potentially related to spring bloom phenology changed after considering tides. Changes include a later onset time of the spring bloom (a), higher peak spring bloom biomass amplitudes (b), a delay in the onset of light conditions in the water column sufficient for phytoplankton growth, as indicated by an integrated light-limiting term in the upper 50 metres exceeds 0.85 (c), the deepening of the mixed layer depth in May (d), a later onset time of stratification, which occurs when the maximum vertical temperature difference in the water column exceeds 0.5°C for three consecutive days (e), and a higher concentration of overwintering zooplankton biomass (f).
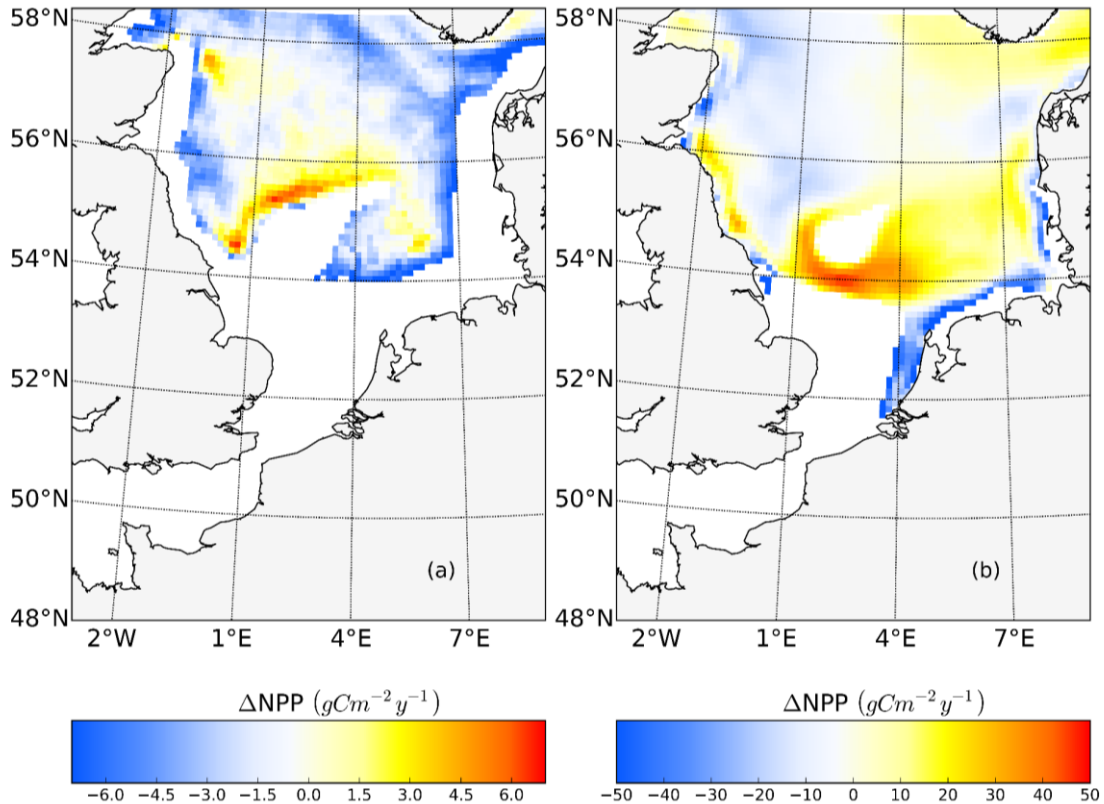
Figure 8. Mean difference in the NPP between the *tidal* and *non-tidal scenarios* generated within the subsurface maximum (SBM) layer (a) and in the surface layer (above 15 metres) (b). The results are averaged for the stratified season. Areas with SBM mean occurrences of less than 10 days per year are excluded in (a). Areas with stratification (squared buoyancy frequency $N^2 >= 0.013$) averaged less than 60 days per year are excluded in (b).
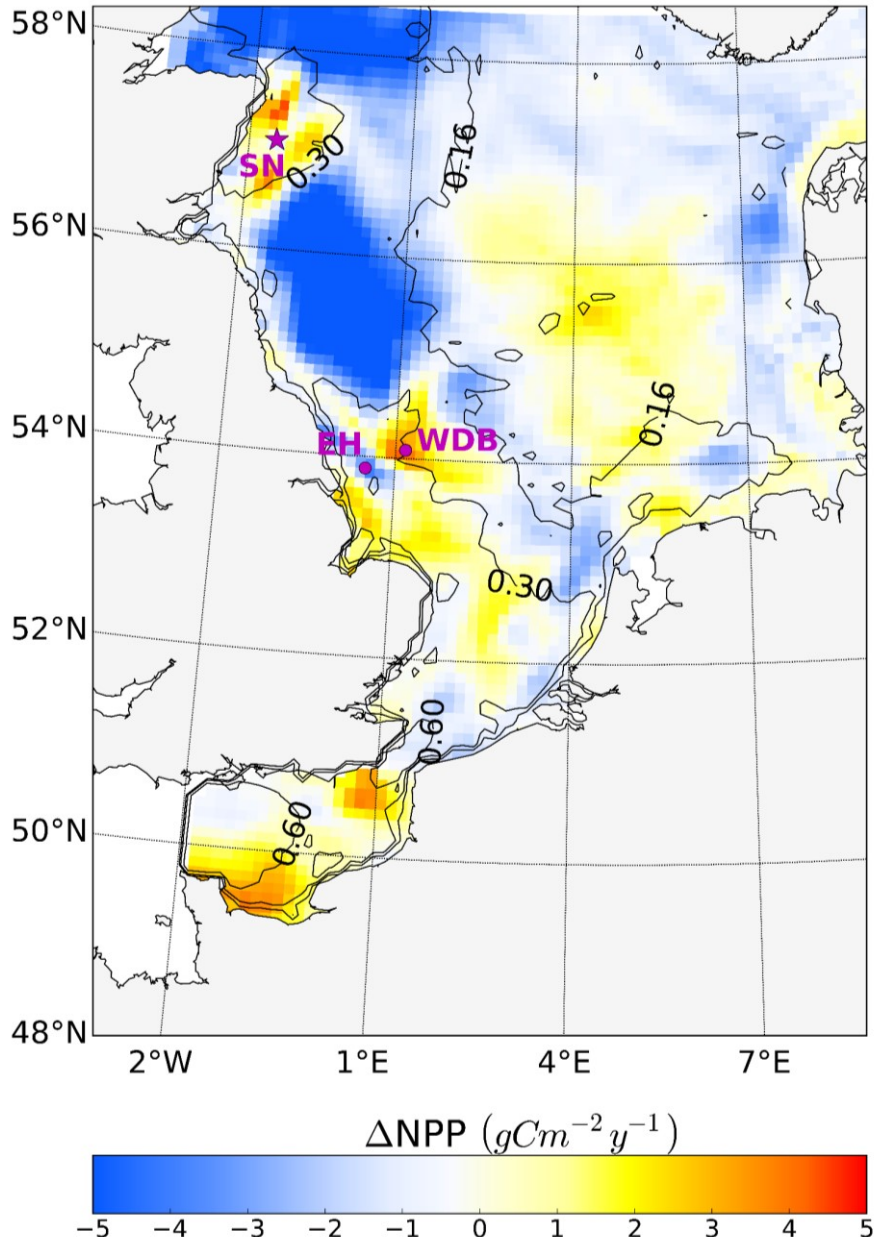
Figure 9. Simulated annual mean NPP difference between the *tidal* (M$_2$ + S$_2$) and *M$_2$ scenarios*, averaged for 1990-2015. Positive values depict higher NPPs in the *tidal scenario* (M$_2$+S$_2$) than in the *M$_2$ scenario*. Contour lines indicate the estimated mean spring-neap cycle range of the tidal current speed difference between the *tidal* (M$_2$ + S$_2$) and *M$_2$ scenarios*. The two magenta dots indicate the locations of 2 characteristic grid cells. One grid cell is close to the Estuary of Humber (EH), and the other grid cell is located more offshore at the western edge of Dogger Bank (WDB) (see Fig. 10). The magenta star shows the location of the grid cell used for the analysis of the advancement and delay of the spring bloom due to spring-neap tidal forcing (see Fig. 11).

Earth System
Dynamics
Discussions
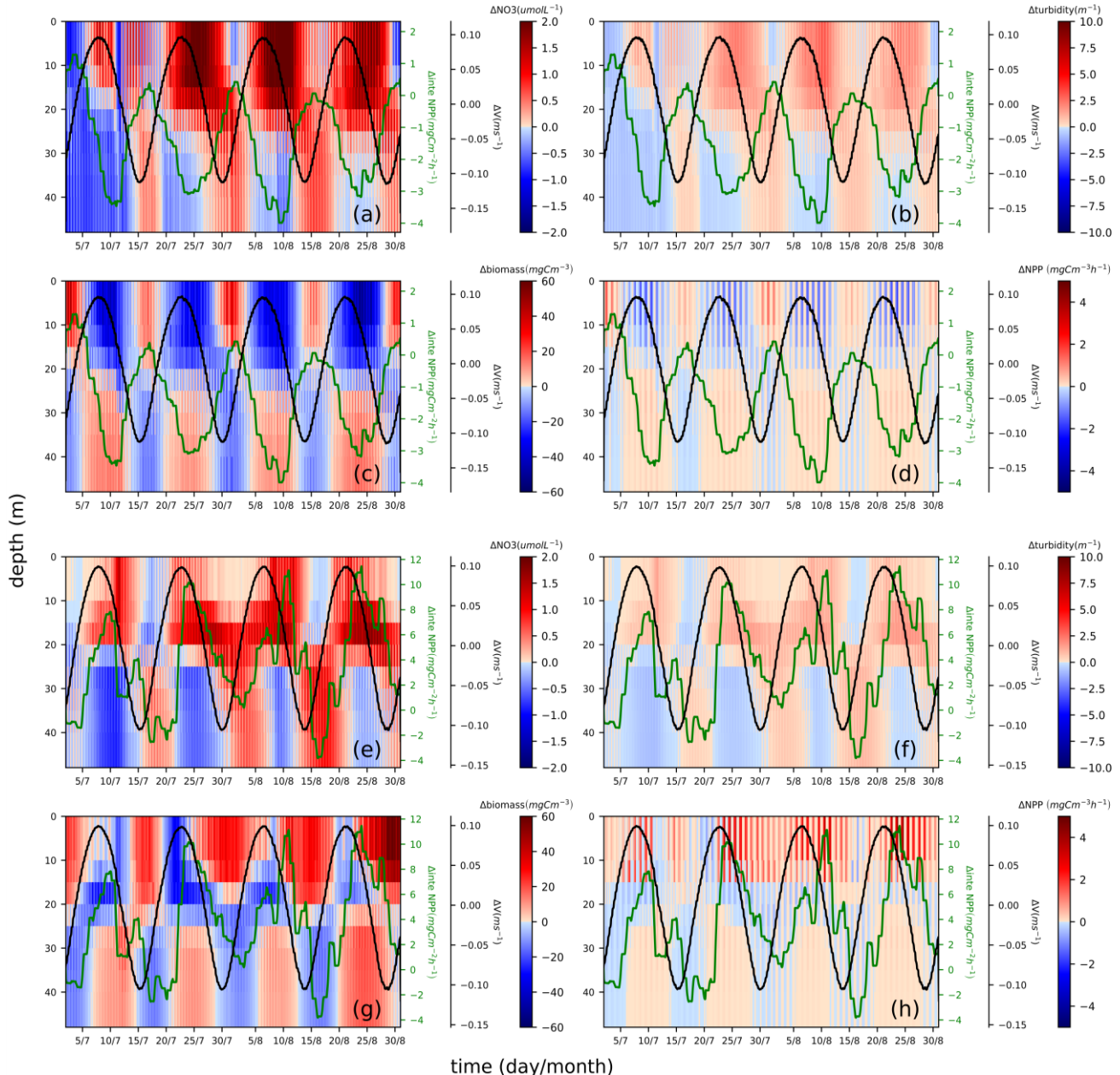
Figure 10. Spring-neap cycle impact on nitrate (a, e), turbidity (b, f), phytoplankton biomass (c, g) and primary production (d, h). Differences between the two scenarios (*tidal scenario* (M₂+S₂) - M₂ *tidal scenario*) are presented for two characteristic points, i.e., EH: upper panel (a, b, c, d), WDB: lower panel (e, f, g, h). To show the periodical fluctuation of currents and NPP and relate these fluctuations to changes in nitrate, turbidity, biomass and NPP, the differences in the depth-averaged velocity amplitude (black) and depth-integrated NPP (green) are presented in each subplot; both time series underwent smoothing with a 24-hour running mean.

1060
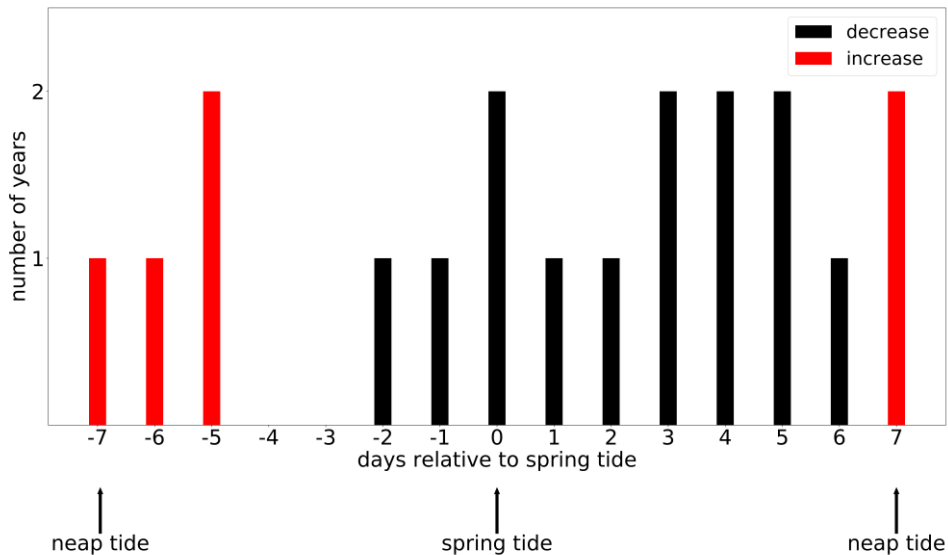
Figure 11. The occurrence of an increase (red) or decrease (black) in the NPP difference (*tidal scenario* (M_2+S_2)-*M_2 tidal scenario*) relative to the nearest spring tide (spring and neap phase indicated). The development of the spring bloom period is defined as the time
1065 when NPP increases from 12.5% to 87.5% of the maximum NPP prior to the major peak of the spring bloom.

1070

1075

1080   **Appendix**
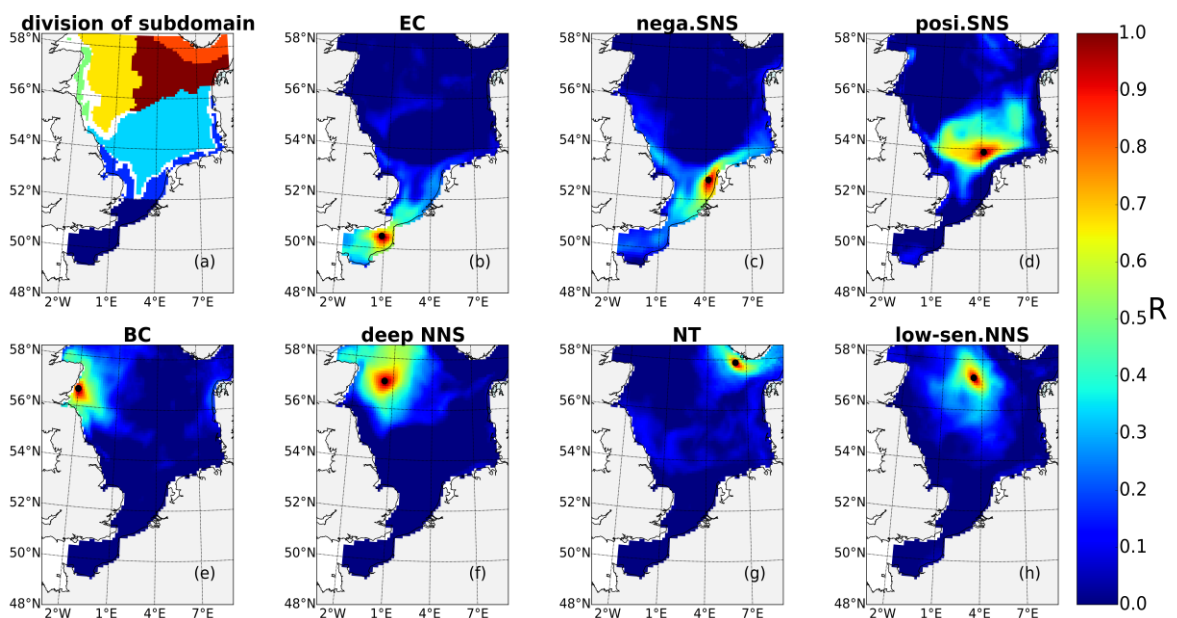
Appendix A. Subdomain divisions (a), correlation coefficient of NPP variations at the most representative grid cell (black
1085   dot) and NPP variations in the surrounding grid cells for the English Channel (b), negatively responding area in the southern
North Sea (c), positively responding area in the southern North Sea (d), the eastern British coast (e), the deeper part of
northern North Sea (f), the Norwegian Trench (g), and the low-sensitive area in the northern North Sea (h).

1090

1095
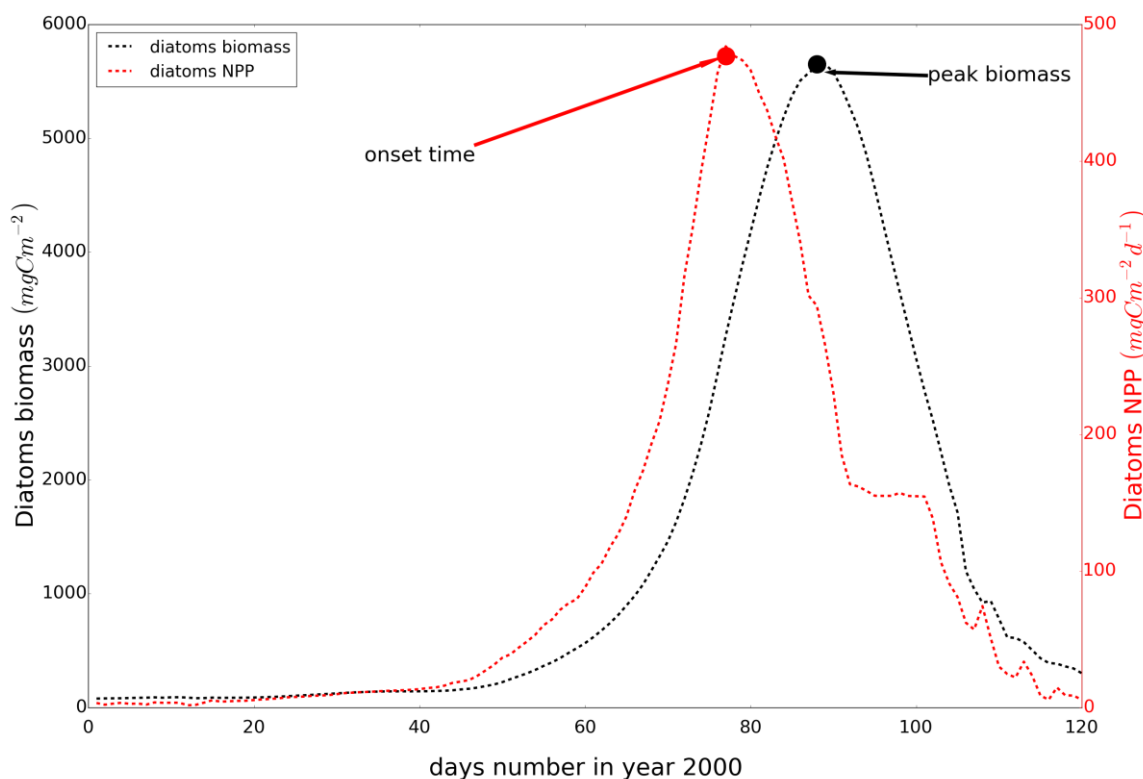
1100 **Appendix B**. The definition of onset time of the spring bloom. The dash black line is the time series of diatoms biomass and the dash red line is the time series of NPP. Both time series have underwent 15-days running average. The black arrow depicts the time when the spring bloom reaches its maximum biomass. The red arrow depicts the time when the NPP reaches its maximum prior to biomass peak, which is defined as the onset time of the spring bloom. The time series is extracted from a grid cell (4.2 °E, 61°N) from the ECOSMO simulation, for the year 2000.

1105
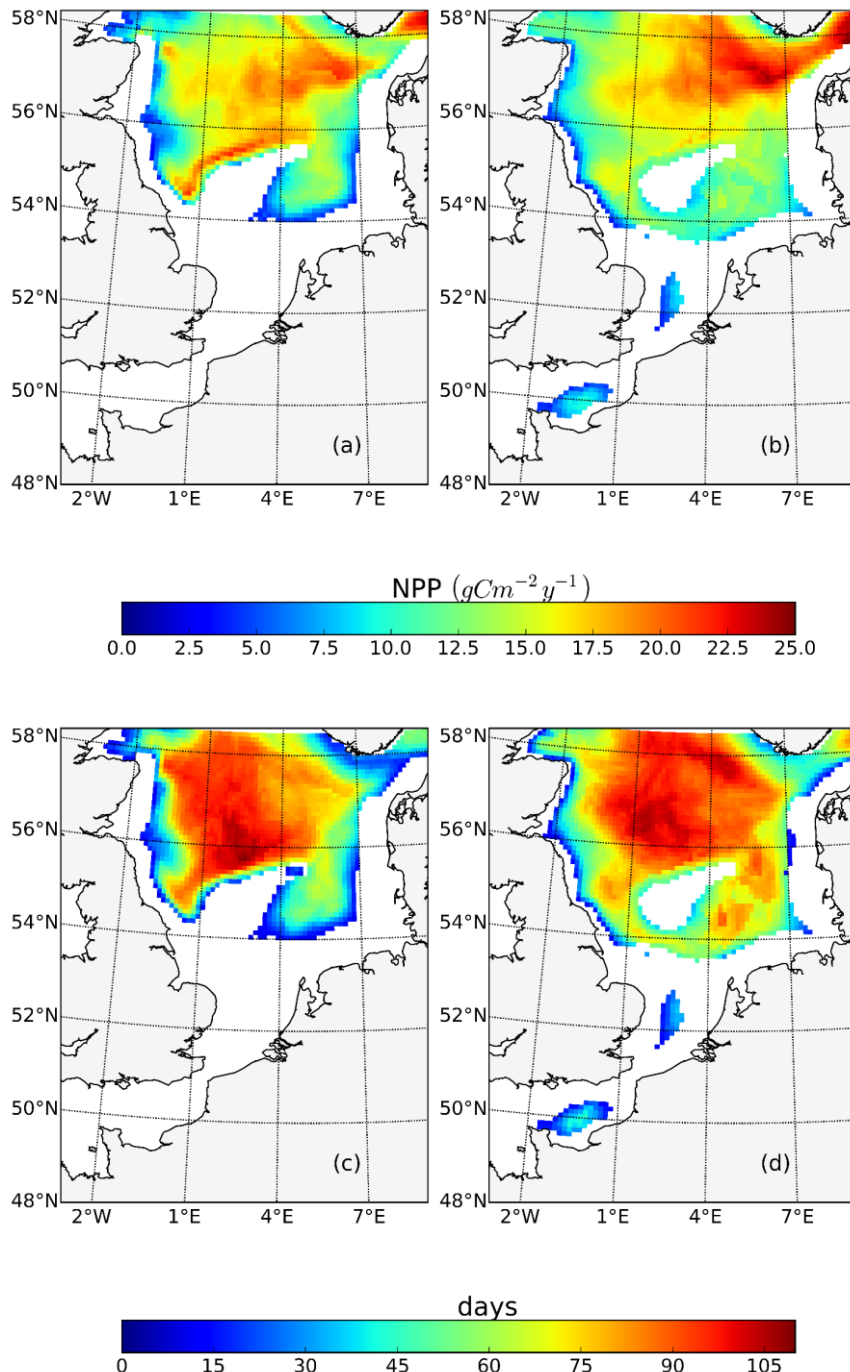
Appendix C. Annual mean NPP contributed by SBM in the *tidal* (a) and *non-tidal scenarios* (b). Survival time of the subsurface biomass maximum (SBM) for the tidal (c) and non-tidal (d) scenarios.